SLOPE STABILITY ANALYSIS OF A SMALL INTERMITTENT FAILURE

A Thesis

Presented

to the Faculty of

California State University, Chico

In Partial Fulfillment

of the Requirement for the Degree

Master of Science

in

Geosciences

Hydrology/Hydrogeology Option

---

by

Chloe Adams

Spring 2015

SLOPE STABILITY ANALYSIS OF A SMALL INTERMITTENT FAILURE

A Thesis

by

Chloe Adams

Spring 2015

APPROVED BY THE DEAN OF GRADUATE STUDIES
AND VICE PROVOST FOR RESEARCH:

_____
Eun K. Park, Ph.D.

APPROVED BY THE GRADUATE ADVISORY COMMITTEE:

_____
Karin A. Hoover, Ph.D., Chair

_____
Gregory R. Taylor, Ph.D.

ACKNOWLEDGMENTS

I wish to express my gratitude for the guidance and support of my advisor Dr. Karin A. Hoover. Input provided by Dr. Gregory Taylor and Dr. Todd Greene have been invaluable in the completion of this project, as well as input provided by Dr. Ann Bykerk-Kauffman, Bill Koperwhats, and Dr. Randy Senock. Financial assistance was provided by grants from the Big Chico Creek Ecological Reserve and the CSU, Chico Research Foundation without which this study would not have been possible. I would also like to thank Greg Adams, Sarah Fein, Nhu Uyen Huynh, Susan Miller, and Bruce Miller for help with the many hours of field work and calculations required for this project.

TABLE OF CONTENTS

LIST OF TABLES

LIST OF FIGURES

FIGURE PAGE

ABSTRACT

SLOPE STABILITY ANALYSIS OF A SMALL

INTERMITTENT FAILURE

by

Chloe Adams

Master of Science in Geosciences

Hydrology/Hydrogeology Option

California State University, Chico

Spring 2015

During significant precipitation events water that does not directly run off infiltrates the soil. If the soils are thin or overlie an impermeable layer, the water will percolate to the impermeable layer and build-up forming a perched water table. If the build-up of infiltrating water generates sufficient pore fluid pressure, the shear strength of the material will be reduced, resulting in slope failure. The objective of this study was to determine the conditions resulting in periodic slope instability on gently sloped terrain. It was hypothesized that that a perched water table, generated by excessive or intense precipitation events, affects the slope stability in the area and results in intermittent movement of the landslide. Data-gathering activities included monitoring precipitation, measuring the height and extent of the perched water table using a piezometer array, interpreting the location and morphology of impermeable boundaries with ground

penetrating radar and assessing relative slide movements. Field measurements suggest that there was a correlation between the amount of rainfall received and the change in height of the rise of water above the impermeable surface; a slope-stability analysis was performed to quantify probable conditions resulting in stability. Conditions that lead to slope instability on gentle slopes in this study were identified as precipitation falling on soils with high antecedent moisture conditions, causing the formation of a perched water table. According to the factor of safety analysis, the height of the perched water table need for movement is met seasonally. Because of the gentle slopes, movement occurred slowly.

CHAPTER I

INTRODUCTION

During significant precipitation events, water that does not directly run off infiltrates the soil. If the soils are thin or overlie an impermeable layer, the water will percolate to the impermeable layer and build-up forming a perched water table. If the build-up of infiltrating water generates sufficient pore fluid pressure, the shear strength of the material will be reduced, resulting in slope failure (Weiler et al., 2006). Although a completely natural phenomenon, slope failures are responsible, on average, for 25 to 50 deaths and in excess of one billion dollars in damages in the United States each year (United States Geological Survey, 2014).

Studies have shown that the formation of a perched water table is a dominant factor contributing to slope instability on steep hillslopes (Torres et al., 1998; Sidle and Swanston, 1982; Leung et al., 2011). A study conducted by Torres et al. (1998) identified hydrologic, weathering, and soil transport controls on shallow landslides and landscape evolution in a steep area of the Oregon Coast Range. It was found that the soil water retention properties had near-zero pressure heads during light but steady precipitation. A sudden increase in rainfall intensity caused slight but fast-moving pressure waves that rapidly displaced existing soil water, causing pore pressure rise and subsequent slope instability. Sidle and Swanston (1982) found that after a storm in which 54% of the precipitation fell in three hours, an increase pore pressure at the slide surface caused

failure of the 43° slope. Leung et al. (2011) found that shallow transient perched water tables developed in colluvial deposits and the main water table rose significantly when the hillslope was subjected to high intensity rainfall. Groundwater flowed along the central portion of the landslide body, resulting in a multiple translational and rotational slide failures. However, there are far fewer studies that focus on the effects of seasonal perched water tables on shallow landslides on gentle slopes. Talebi et al. (2008) created a probabilistic rainfall- induced shallow landslide model and applied it to complex hollows. Model results suggested that on gentle slopes, an increase in colluvium thickness increased hillslope stability.

It is known that surface and subsurface topography greatly influence the formation of perched water tables. Steeply sloped land generates faster runoff and less infiltration than gentle slopes; more infiltration on gentler slopes can lead to an increase in saturated soils (United States Geological Survey, 2014). Hillslope hollows at the surface can often concentrate flow paths leading to the generation of perched water tables and thus increasing landslide susceptibility. Anderson (1982) reported that only in soils with high hydraulic conductivity on steep slopes does subsurface flow concentrate in hillslope hollows and form perched water tables. In situations with lower hydraulic conductivity on more gentle slopes, flow paths were shown to migrate across hollow-spur topography (Anderson, 1982). In cases where bedrock topography differed greatly from surface topography, subsurface storm flow paths followed bedrock topography rather than surface topography (Freer et al., 2002).

The objective of the current research is to analyze the volume and intensity of the precipitation and the surface and subsurface topography promoting the on-going

movement of a shallow rotational failure using a combination of field measurements and modeling. The landslide is located in northern California, in the lower portion of the Big Chico Creek watershed in Butte County (Figure 1). The site was selected because it is an

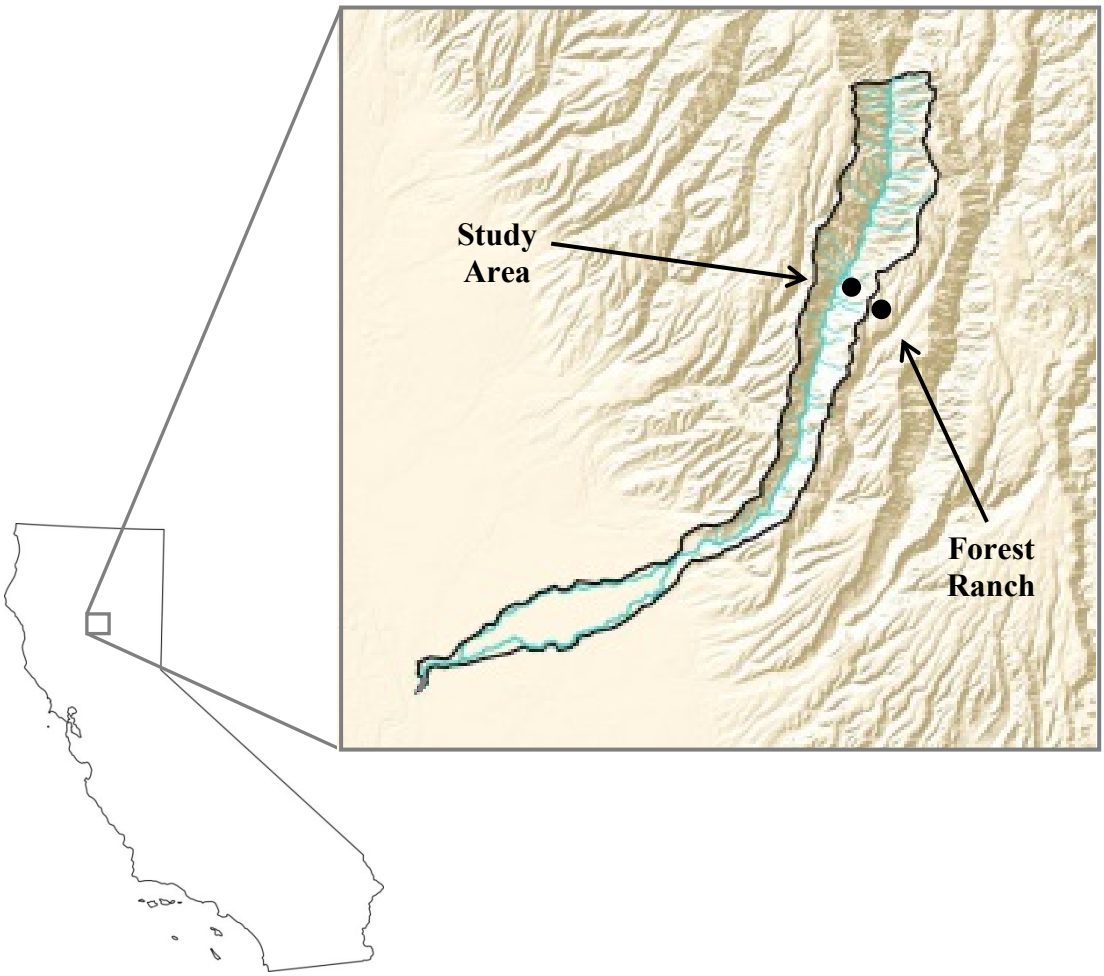

Figure 1. **Location map of the study site showing the location in relation to Forest Ranch and the Lower Big Chico Creek watershed boundary, California.**

ideal location for studying the effects of seasonal, transient water tables on the stability of low slopes. Surface flow and evidence of subsurface flow are visible in several areas in and around the landslide. The landslide moves intermittently and is actively delivering

sediment to the creek. The landslide is easily accessible via the road that goes through it. The road has failed twice, once in late February or early March of 1998 and again two to three years later. The property owner witnessed the first event and described the antecedent moisture conditions of the soil as saturated after a fair amount of rain. “A small crack started in the road and within 3 hours the slide had moved enough that the road was impassable. The top layer of earth slipped off another layer underneath [and I had] the thought that the water couldn’t penetrate the lower layer” (D. Schroeder, personal communication, May 1, 2014).

The hypothesis to be tested was that a perched water table, generated by excessive or intense precipitation events, affects the slope stability in the area and results in intermittent movement of the landslide. The location, as well as the horizontal and vertical extents of the perched water table, were expected to be influenced to a large degree by the surface and subsurface topography within the study area. Data collection activities included gauging precipitation, analyzing piezometric data, mapping surface and subsurface topography and monitoring the distance the landslide moved over a one-year period. A rain gauge was used to determine precipitation amounts. Five piezometers were placed in the body of the slide and fitted with pressure transducers to measure the height of the water table. Surface slope maps were generated using on-the-ground mapping techniques and ground penetrating radar was used to identify any underground features such as slide planes, impermeable boundaries, or perched water tables. Survey flags were placed in several locations at the top and bottom of the landslide scarp and the distances between them were measured to determine movement, if any. Data were collected after big precipitation events.

The expectation was that during intense and extended rainfall events, infiltration of water into the soil would cause saturated conditions resulting in the build-up of pore fluid above relatively impermeable bedrock. Positive pore fluid pressures would then reduce the shear strength of the soil and allow for potential grain buoyancy, causing the slope to become unstable and subsequently to fail. Analysis of the data indicated that when seasonal precipitation amounts exceeded a critical threshold, a perched water table formed at the toe of the failure and moved upslope with each additional storm. The depth of the perched water table varied from six inches deep directly after precipitation events to greater than six feet deep during periods without precipitation throughout the monitored period. The ground penetrating radar survey revealed two impermeable layers creating a surface for a perched water table as well as defining the relative shape of the rotational failure. While slide movement data were inconclusive, measurement of the tilt of the piezometers indicated that the slide was actively moving. A factor of safety analysis suggested that the slope becomes unstable when the sliding material is saturated to a distance halfway between the impermeable bedrock and the surface, a condition that occurs frequently during seasonal precipitation.

CHAPTER II

SITE DESCRIPTION

Investigations analyzing the effects of a perched water table, surface topography and depth to impermeable bedrock of an intermittent shallow rotational failure were undertaken on a site located near Forest Ranch, California approximately 16 miles east of from Chico, California. The study site is located in the Big Chico Creek watershed at a latitude of 39°52'53.66" N and a longitude of 121°42'3.78" W (Figure 1) and an elevation of 1000 ft. The size of the site is approximately 3.1 x 10^4 m^2. A gravel road passes through the landslide on the east. Intermittent movement on the slide has caused sections of the road to fail twice; the sections have been fixed using rip rap to add stability and decrease erosion. Movement of the slide also delivers an unknown quantity of sediment into Big Chico Creek.

The area has a Mediterranean climate receiving most of its precipitation predominantly in the winter followed by hot, dry summers. The coldest month is December, the warmest month is July, the wettest month is January, and the driest month is July. Temperatures in the region average 54.0°F, ranging from 40.0°F to 92.0°F. The average precipitation is 40.3 inches per year, ranging from 21.04 to 67.44 inches. Most of the precipitation that occurs in the study area falls as rain (California Department of Water Resources, 2012).

The geologic materials that underlie the site area are the Chico Formation and older landslide deposits. The Chico Formation is a Late Cretaceous (65-75 ma) age medium-grained marine sandstone, visible in scarps in a larger landslide east of the study area, as well as on the incised channel of Big Chico Creek. The Tuscan Formation unconformably overlies the Chico Formation can be seen in the region as cliff-forming layers. The Tuscan Formation is a Late Pliocene (2.8-3.3 ma) unit composed of volcanic mud flow and volcanic sedimentary layers (Olmsted and Davis, 1960). The older landslide deposits in the study area are composed of both Chico and Tuscan formations.

Soils in the study area are vary as a function of parent material and slope; 42% of the soils consist of ultic haploxeralfs, on 3 to 15 percent slopes and 58% consist of Chinacamp gravelly loam on 15 to 30 percent slopes. The ultic haploxeralfs soils occupy the northern and central sections of the study area. The soils are derived from sandy colluvium and/or residuum from weathered sandstone. The typical profile consists of very fine sandy loam from 0 to 24 inches, very gravelly very fine sandy loam from 24 to 32 inches, and very gravelly sandy clay loam from 32 to 53 inches where it is in contact with paralithic bedrock. The Chinacamp gravelly loam occupies the western and southern portions of the study area. The parent material is a stony fine-loamy colluvium derived from volcanic breccia. A typical profile consists of 0 to 1 inch of slightly decomposed plant material, 1 to 5 inches of gravelly loam, 5 to 44 inches of gravelly clay loam, 44 to 61 inches of extremely stony clay loam and 61 to 72 inches of very stony clay loam. The depth to a restrictive feature is more than 80 inches (Natural Resources Conservation Service, 2015).

Vegetative cover consists of grassland, hardwood trees, and various shrubs. Tall to medium grasses are seen throughout the site but are concentrated at the northern side of the site; shorter, more marsh-like are grasses are located near areas of ponded or subsurface flow and make up approximately 35 % of the study area. Oak trees dominate the landscape and contribute 45% of the vegetative cover. Shrubs including milkweed, poison oak, blackberries and others make up 15 %. Artificial cover including the gravel road shoulder and rip rap used to hold road in place from previous road failures, make up the remaining 5% of the study site.

The rotational failure occupies approximately 1.25×10^4 m^2 on the west side of the study area and exhibits a variety of slopes and surface features. Slopes directly above the failure headwall and graben (trench) range between 15° and 18° (Figure 2). Just west of the road slopes increase to 26°-30°, and further west an angular concave slope break gives way to gentile 8°-13° slopes. A smooth concave slope break parallel to the creek results in slopes between 2°- 8° from the break to the drop off into the creek. The edge of the creek is a steep (greater than 40°) slope composed of soil and rock. The graben is well defined on the north and east sides but is broken and begins to dissipate to the southeast. The northern section of the graben, on the west side of the road, varies in depth and width from 0.2 m deep and 1.0 m wide near Big Chico Creek to 2.0 m deep and 6.0 m wide near the road. This section is situated in thinner sandy soils that form 0.25 to 0.50 m terracettes lining the interior walls of the graben. The eastern section of the graben has an arcuate shape and is not continuous on the upper central side of the slope. Width of the graben is approximately 8 m on the east side of the road excluding the

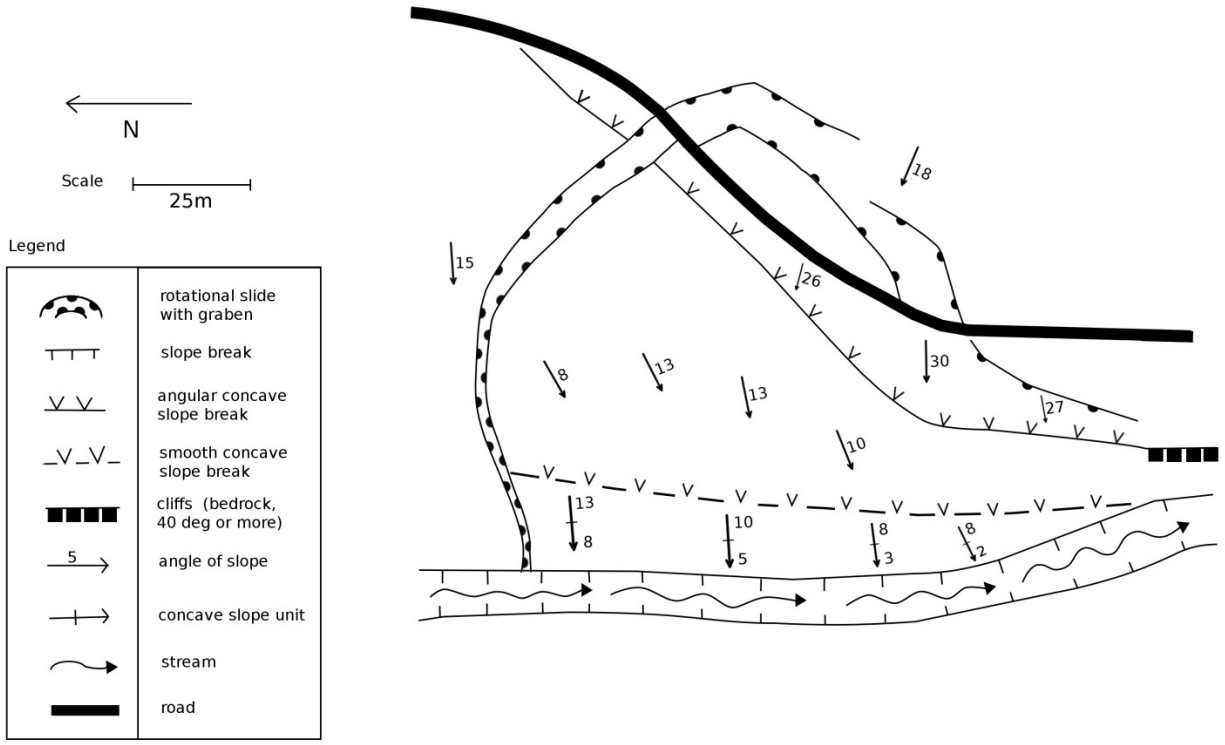

Figure 2. Slope map of the study area depicting a landslide, graben, road and slope features.

fragmented portion. The depth varies greatly from 2.5 m on the northeast side to 1.0 m to the southeast.

Ephemeral drainage occurs during November through June and can be seen in the shallow soils just above the slide, as micro and macropore flow caused by small animal holes north-east of the slide, and in a marshy area within the southwest section of the slide. Several areas of ponded water are visible northwest of the site as well as many areas of surface and subsurface flow. On the south side of the slide there is flow visible on the surface as well as several shallow marshy areas.

CHAPTER III

METHODS, INSTRUMENTATION AND RESULTS

To investigate the conditions generating intermittent slope failure, a rain gauge was installed to monitor precipitation and an array of piezometers fitted with pressure transducers were used to record the height of the perched water table. The slope map was used to determine if the location and extent of the perched water table was governed by surface topography or if the build-up of soil water followed the subsurface topography; a ground penetrating radar survey was used to determine the subsurface topography and the depth to an impermeable layer. Because movement measurements made using pin flags were inconclusive, measurements of piezometer tilt provided directional movement data.

To gauge precipitation inputs to the study area, a standard rain gauge was placed in a central location within the landslide free of shrubs and trees. The rain gauge was attached to a metal pipe using plastic zip ties, approximately one foot above grass height. The gauge was checked after precipitation events and several problems were encountered. The first problem was that the gauge did not hold an adequate volume of water to capture total precipitation amounts between readings. The second problem occurred when twigs and leaves from a nearby frequently fell into the gauge and displaced the water. The third problem was possible animal activity; the gauge was

knocked over on one occasion and broken off of the post on another. Therefore, alternate rainfall data were acquired. Hourly precipitation data from October 4, 2009 to October 3, 2010 were obtained from the Cohasset weather station, located at latitude 39.875278°N, longitude 121.770554°W, at an elevation of 1600 feet. This station is approximately 6 km west and 600 feet higher in elevation than the study area.

The data indicate that there were nine significant precipitation events that occurred between October 4, 2009 and October 3, 2010. For the purposes of this study a significant event is defined as precipitation greater than 1 inch with 24 hours of no precipitation between events. This was done to eliminate smaller precipitation events that would not directly contribute to the build- up of the saturated zone above the failure plane. Event 1 was an 18-hour storm that delivered 2 inches of precipitation, with a maximum intensity of 0.25 in/hr., after a 30 day dry period (Figure 3). Event 2 lasted 78 hours with a maximum rainfall intensity of .28 in/hr.; the cumulative precipitation for the storm was 3.74 in. Event 3 was spilt into two sub-events; Event 3a lasted 8 hours and delivered 1.15 inches of precipitation with a maximum intensity of 0.24 in/hr. Event 3b dropped 0.68 inches of precipitation during a 12 hour period with a maximum intensity of 0.43 in/hr. The first part of the event had less intense rainfall; the second saw most of the precipitation in one hour. Event 4 was a series of storms lasting 9.5 days. The accumulated precipitation was 10.72 inches and the maximum rainfall intensity was 0.48 in/hr. Event 5 was split into two sub-events. The duration of these events were both 16 hours. Total precipitation for event 5a was 1.23 inches with a maximum intensity of 0.15 in/hr. Total precipitation for event 5b was 0.96 inches with a maximum intensity of 0.15 in/hr. Event 6 lasted for 23 hours, had a total of 1.33 inches of precipitation, and had a

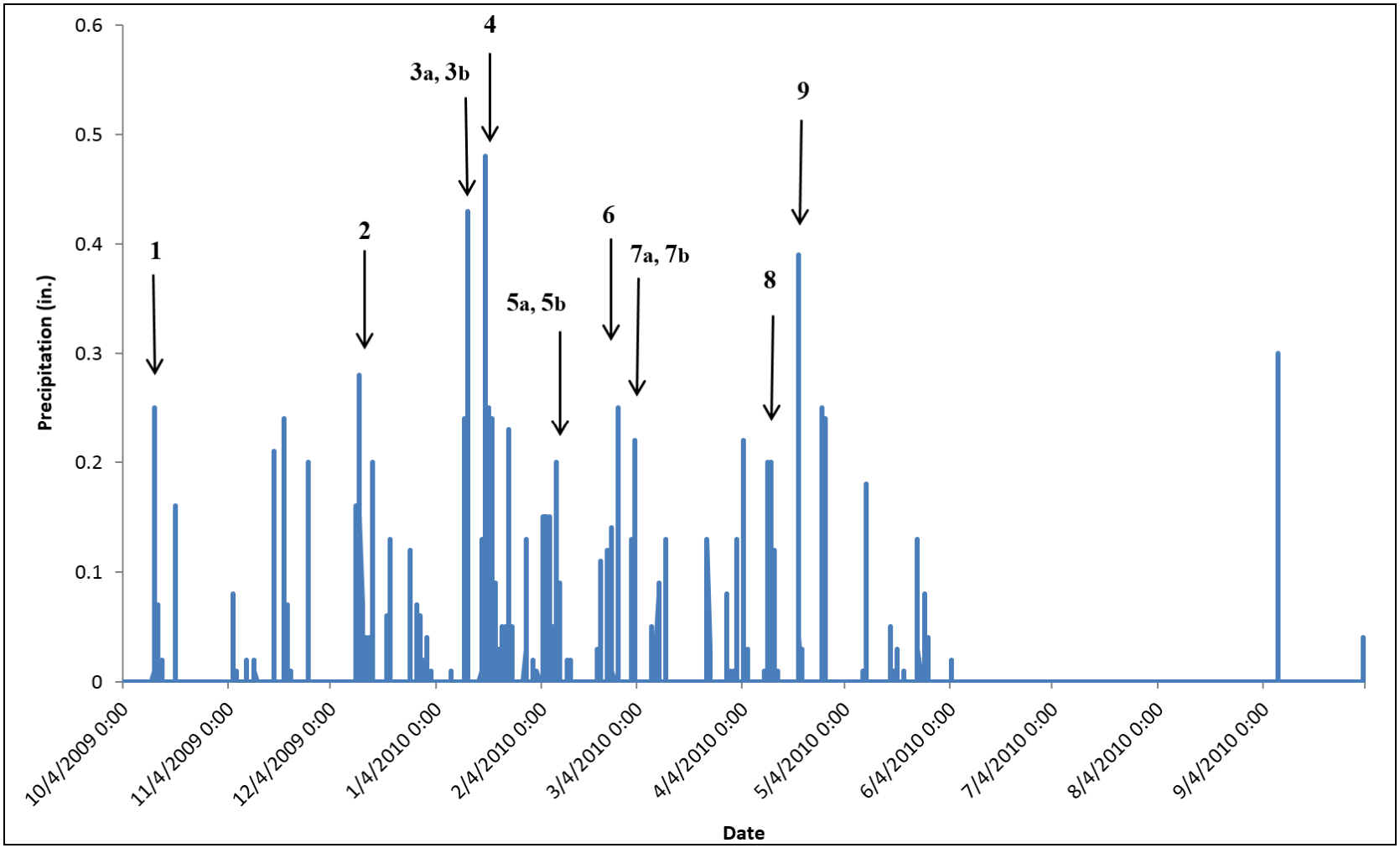

Figure 3. Precipitation events from October 4, 2009 to October 3, 2010.

maximum intensity of 0.14 in/hr. Event 7 was separated in to two sub-events. Event 7a lasted for 10 hours with a maximum intensity of 0.13 in/hr. and delivered 0.37 inches of precipitation. Event 7b lasted for 5 hours, had a total of 0.81 inches of precipitation, and a maximum intensity of 0.22 in/hr. Event 8 had a total of 2.84 inches over a 50 hour period, with a maximum intensity of 0.16 in/hr. Event 9 had 2 inches of precipitation over 32 hours and a maximum rainfall intensity of 0.39 in/hr.

Event 7b lasted for 5 hours, had a total of 0.81 inches of precipitation, and a maximum intensity of 0.22 in/hr. Event 8 had a total of 2.84 inches over a 50 hour period, with a maximum intensity of 0.16 in/hr. Event 9 had 2 inches of precipitation over 32 hours and a maximum rainfall intensity of 0.39 in/hr.

Hypothesized to occur each winter, during the study period a perched water table formed at the base of the rotational failure above an impermeable surface. To monitor the response of the perched water table to precipitation events, an array of five piezometers was installed in locations evenly distributed across failure (Figure 4). Four piezometers were located within the landslide and one was placed near the north eastern side just outside the failure. A sixth piezometer was not fitted with a data logger because adequate soil moisture content was not encountered while digging the emplacement hole to warrant monitoring equipment.

Installation methods were similar for all piezometers. Piezometers holes were dug using a three-inch diameter auger. The piezometer holes were deepened until saturated soil was reached (Table 1). Two inches of RMC 40 Lonestar sand was placed at the bottom of each hole. Two inch diameter PVC pipes with 10-inch slotted sections at the bottom were inserted into the hole to create the piezometer. Approximately 12 inches

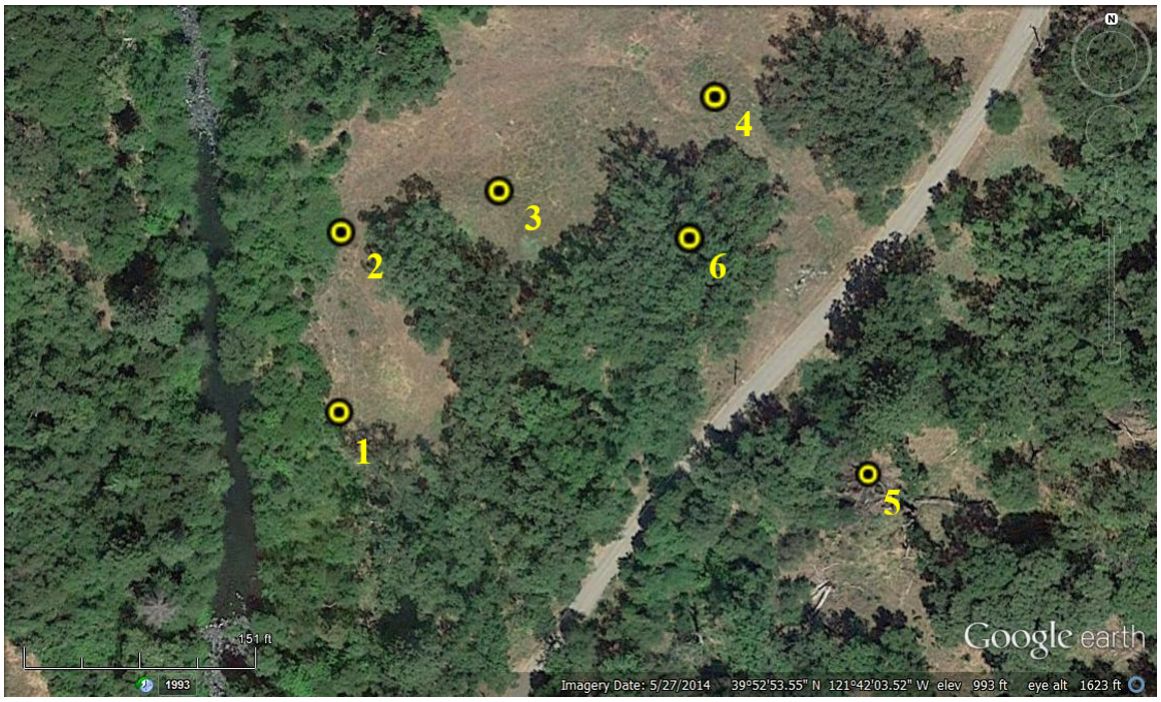

Figure 4. Locations of the piezometers within the study area.

Source: "Piezometer locations." 39°52'53.55" N and 121°42'03.52" W. Google Earth. May 27, 2014. October 07, 2014.

TABLE 1. DEPTHS OF PIEZOMETERS IN THE STUDY AREA

Piezometer	Depth (inches)
1	49
2	65
3	67
4	48
5	54
6	165

of sand was filled around the bottom of each pipe to aid in drainage and filtration of the piezometer. Soil was then back-filled into each hole until it reached six inches from the ground surface. Seven inches of bentonite pellets were filled to the top of the hole and slightly mounded to prevent precipitation from seeping around the sides of the piezometer.

Pressure transducers attached to data loggers were installed in the piezometers to gauge the fluctuation of water levels before, during and after storms. Data were recorded hourly from October 4, 2009 to October 3, 2010. Piezometers 1 through 4 were outfitted with HOBO Water Level Loggers. Because these are absolute pressure loggers, a barometric pressure sensor (HOBO Micro Station) was used nearby and HOBOware software was used to convert these measurements into water levels. Piezometer 5 contained a Global Water WL15 Water Level Logger. This data logger is a vented pressure transducer connected by a 25-foot cable. Because the cable didn't fit in the piezometer it was coiled next to it and wrapped in plastic sheeting to prevent moisture or precipitation from entering the piezometer or data logger. On two occasions animals had ripped the plastic sheeting and possibly allowed precipitation to enter the piezometer. On the second occurrence the data logger was removed to prevent damage to the equipment. Data suggested that there was no change in water level during the recorded period.

Changes in height and extent of the perched water table in response to precipitation events, as recorded by the piezometer array, varied as a combination of piezometer location, storm intensity, antecedent moisture conditions and sensor malfunction.

Piezometer 1, located in the toe of the failure on a small hummock (Figure 4) was the least responsive of the sensors; water levels in the piezometer ranged from 0.0 to 2.9 feet with high levels corresponding to three of the nine events. The piezometer also exhibited a high water level during a storm not considered a significant event according to the criteria set forth earlier. A water level of 2.6 feet corresponded to the period of greatest rainfall intensity during precipitation event 4 (Figure 5); the piezometer then

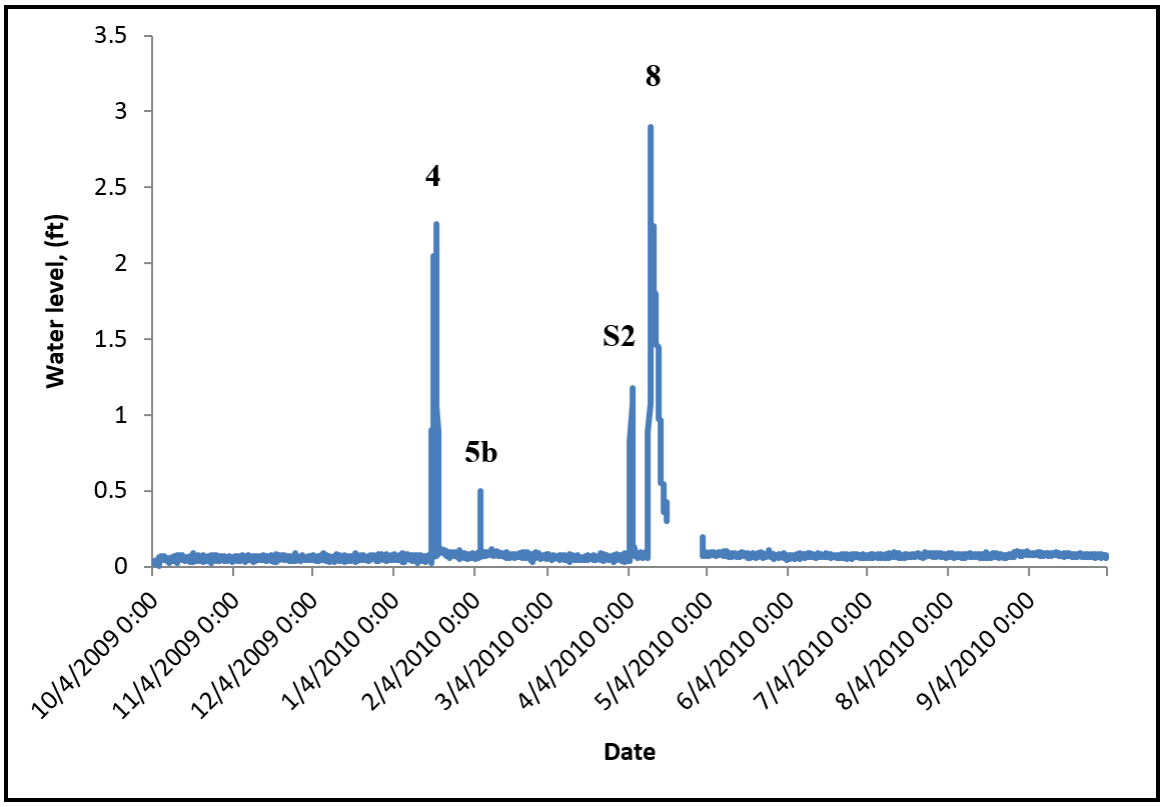

Figure 5. Water levels in piezometer 1 and corresponding precipitation events.

drained rapidly before the event finished. A water level of 0.5 feet was exhibited during event 5b. High antecedent moisture conditions produced by event 5a and maximum rainfall intensity for the 5b event likely contributed to this increase in water level. A

water level of 1.2 feet did not correspond to a designated precipitation event because the storm (S2) did not produce one inch of precipitation, although it did produce a sustained average rainfall intensity of 0.20 in/hr. for 3 hours. The fourth and final water level on the graph corresponded to precipitation event 8. With a water level of 2.9 feet, it was the highest of all responses and the piezometer did not drain as quickly as after the other events. Unfortunately, the sensor was mistakenly turned off for the latter portion of this last event and the response of Piezometer 1 during event 9 was not captured. From the data available, it appears that the response of Piezometer 1 was governed by rainfall intensity and antecedent moisture conditions rather than the amount of precipitation during any single storm event. The lack of response to most of the storm events is probably due to its location on a small mound near the edge southern edge of the slide. It is possible that the slight elevation of Piezometer 1 was just high enough to only capture the higher water table levels.

Piezometer 2, located in a swale on the west side of the failure near Big Chico Creek (Figure 4), exhibited a response to all of the precipitation events and maintained water from January 12, 2010 to July 1, 2010. A water level of 0.9 feet corresponded to precipitation event 1 (Figure 6); Piezometer 2 was the only piezometer to register the event. A water level of 1.1 feet corresponded to the highest rainfall intensities for precipitation event 2 and a water level of 3.2 feet corresponded to the peak rainfall intensity for event 3b. After this event a permanent perched water table was formed. High water tables were recorded for events 4, 5b, and 6 with a peak water level of 5.3 feet corresponding to precipitation event 8. The response of Piezometer 2 to precipitation

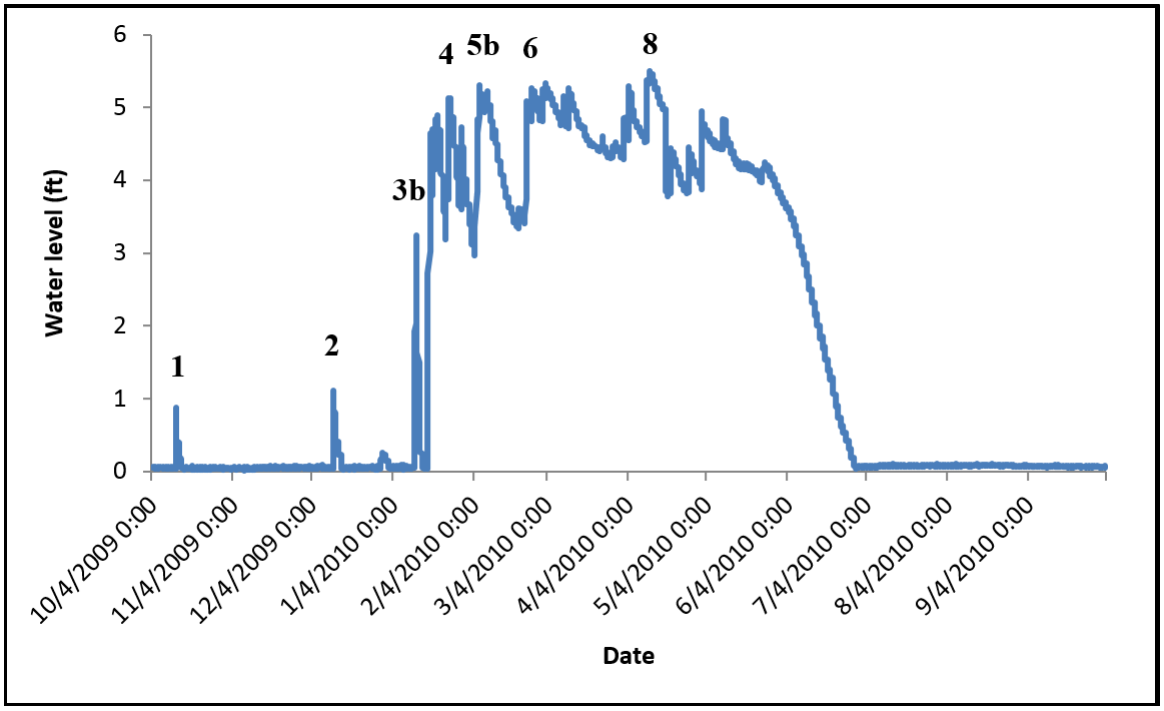

Figure 6. Water levels in piezometer 2 and corresponding precipitation events.

events can be attributed to its location in a swale near the edge of Big Chico Creek that collected and infiltrated precipitation.

Piezometer 3, located in the northern third of the slide between the road and the creek on a mild 13° slope (Figure 4), maintained water from January 18, 2010 to June 15, 2010. Water levels ranging from 0 feet to 4.7 feet in Piezometer 3 corresponded to precipitation intensity peaks for events 4, 5b, 7b, and 8 (Figure 7) with the highest peak of 4.7 feet occurring on March 3, 2010 during precipitation event 7b. High water levels also occurred during precipitation events on March 10, 2010 (S1) and April 4, 2010 (S2), although the storms occurring on those dates did not produce enough precipitation to be considered significant events, producing 0.8 inches in 5 hours and 0.9 inches in 7 hours, respectively. High water levels and the formation of a more permanent perched water

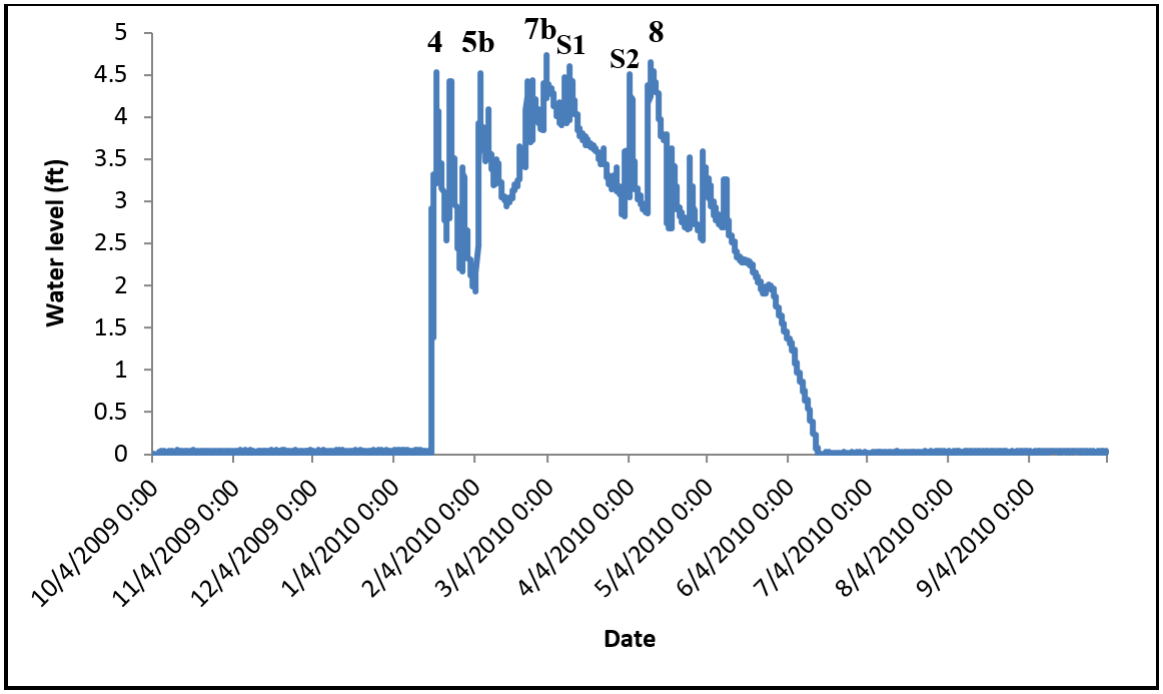

Figure 7. Water levels in piezometer 3 and corresponding precipitation events.

table were probably the result of Piezometer 3 being located near a slope break where surface water could accumulate and aid infiltration.

Piezometer 4, situated in shallow soils just outside of the north end of the landslide (Figure 4), exhibited a perched water table from January 20, 2010 to April 26, 2010 and then again from April 27, 2010 to May 27, 2010. High water levels of 0.8 and 2.0 feet occurred during precipitation event 4, a series of storms lasting 9.5 days (Figure 8). These storms produced enough precipitation to create a sustained perched water table. The high water level of 2.9 feet during precipitation event 5b did not correspond to peaks in rainfall intensity, unlike water levels of 2.7 and 2.8 feet during events 7b and 8, which did correspond to increases in rainfall intensity. The high water level recorded on May 2, 2010 corresponded to a brief 2 hour storm (S3) that occurred 4 days earlier. The

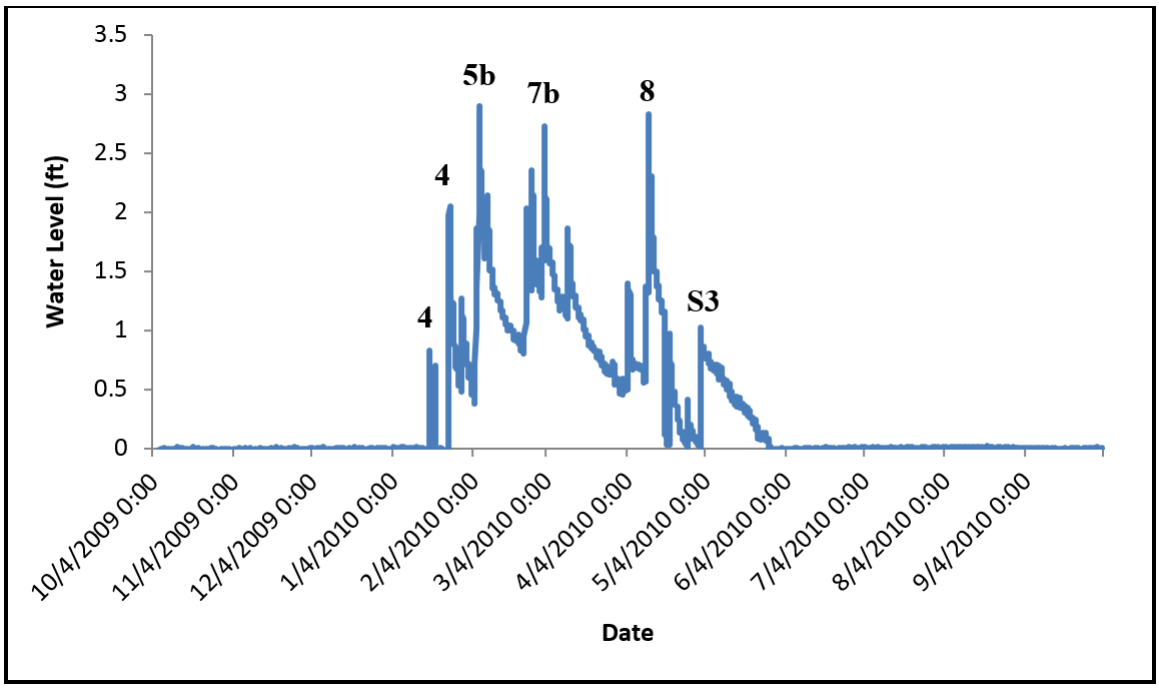

Figure 8. Water level in piezometer 4 and corresponding precipitation event.

piezometer was located in thin soils just outside the failure on a slope dipping 15° west toward the creek. This allowed for more runoff and less infiltration due to its placement on the slope.

When examining the piezometer data some similarities and differences became evident (Figure 9). Located near the creek on the south side of the study area, Piezometer 1 was the least responsive of all the piezometers and drained quickly. Piezometer 4 was the second least responsive of the piezometers but was able to maintain a water level from January 20, 2010 to April 26, 2010 but drained more quickly than Piezometers 2 and 3. Both Piezometers 1 and 4 were at similar depths, 49 and 48 inches respectively, and were placed in fine sandy loam; however, Piezometer 1 was located on a small hummock near the creek and Piezometer 4 was on a 15° slope just outside of the failure to the north. Piezometers 2 and 3 were 65 and 67 inches deep respectively and

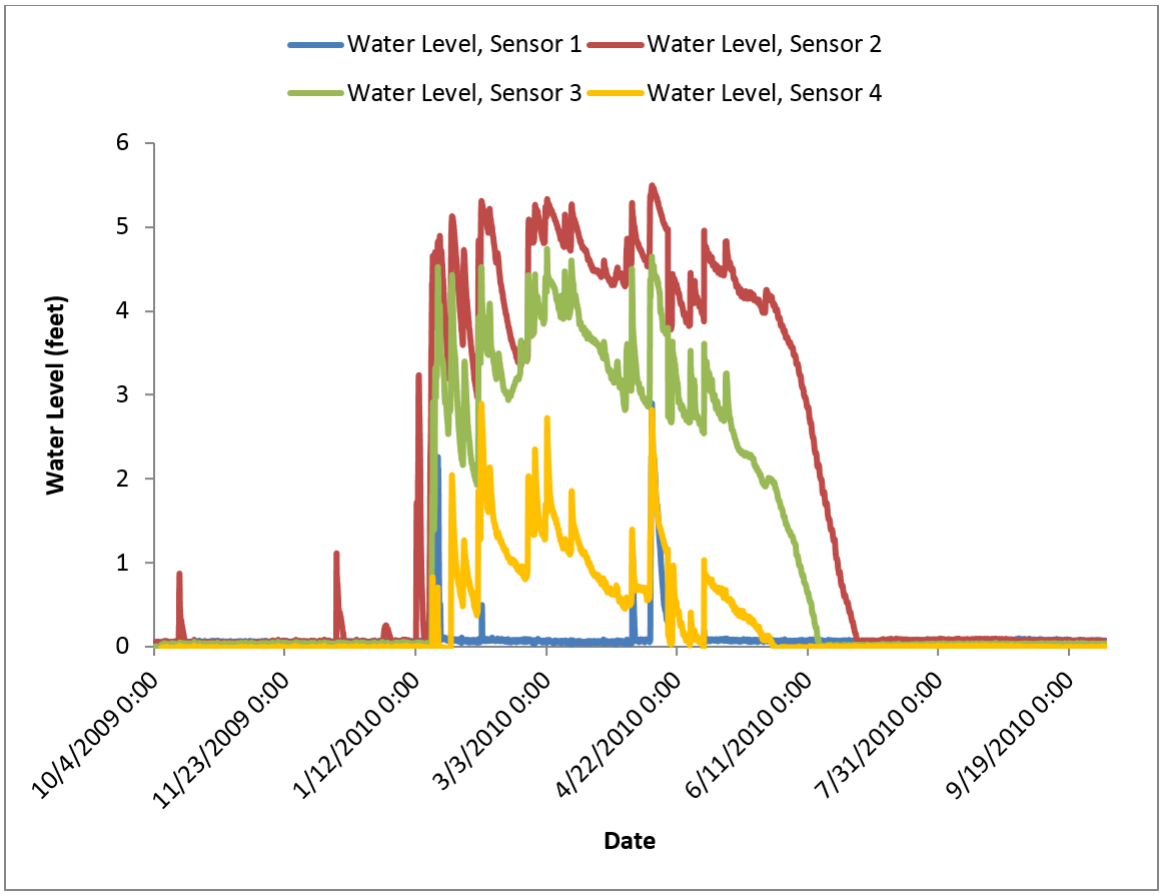

Figure 9. Water levels in piezometers 1-4.

responded similarly to precipitation events with Piezometer 2 being the most responsive of the all the piezometers. Piezometer 2 was located near Big Chico Creek in a swale and had a perched water table for the longest period of time while Piezometer 3 was located in the northern third of the slide between the road and the creek on mild 13° slopes.

Ground penetrating radar (GPR) was used to investigate subsurface features such as the elevation of the perched water table, the location of failure surfaces and subsurface topographic features contributing to slope instability.

A pulseEkko 100 ground penetrating radar was used to perform a common offset reflection survey. One hundred frequency (MHz) antennas were used with an 0.25

meter step size and a 1 meter antenna separation. One hundred MHz geophones were used because the landslide was thought to be relatively shallow (<25 m) deep based on exposed bedrock and areas of ponded water around the edges of the study area. The wave velocity was set at 0.1 m/ns based on the average velocity of geologic materials. The time window was calculated automatically using based on the chosen velocity. Because of heavy tree cover and thick vegetation, locations where an accurate survey could be performed were limited. Three locations were chosen throughout the study area (Figure 10). Line 1 was near the middle of the slide on the main road running south-southwest. This area was clear of brush and relatively clear of overhead foliage. This location was not ideal, as it was below overhead utility lines. Line 2 was near the south edge running

Figure 10. Satellite photo showing ground penetrating radar transect locations.

Source: "Ground penetrating radar transect locations." 39°52'53.54" N and 121°42'02.91" W. Google Earth. May 27, 2014. October 08, 2014.

nearly perpendicular to the other lines. This line had the most overhead coverage but there were few options in the northwest direction free of brush. Because of its unnatural uniform slope, this line may have been situated on an old unmaintained steep dirt road. Line 3 was in the lower third of the slide running southwest through the site. While there was partial tree cover and possible root interference, this line crossed the graben, and was near a ponded area and an open flat area.

Despite difficulties encountered during the surveys, primarily associated with maintaining equal and level spacing of the instrument's skis, the three lines surveyed produced interpretable images composed of strong, medium strength and weak reflectors.

Line 1, located along the road and running northeast to southwest, was 80 m long and penetrated to a depth of approximately 13 m (Figure 11). All three types of reflectors were visible in this line. The first reflector was strong and encompassed more than half of the GPR line, beginning at the start of the line and pinching out at 64 m distance at a depth of 7 m (Figure 12). The associated reflections were stronger and more chaotic near the surface, gradually weakening with the depth. Because there were several jumbled interbedded reflections within this section, separation of the surfaces was difficult. The second type was weak reflector beginning at 36 m, near the surface, and gradually thickens from 0.5 m to a maximum of 7 m. It was smoothly textured, with only minor reflections. The third reflector began 35 m along the line at a depth of 13 m increasing to a maximum thickness of 6 m at 70 m and declining to 4 m at the end of the line. There were two distinct reflections within this section with smaller parallel medium-strength reflections beneath them.

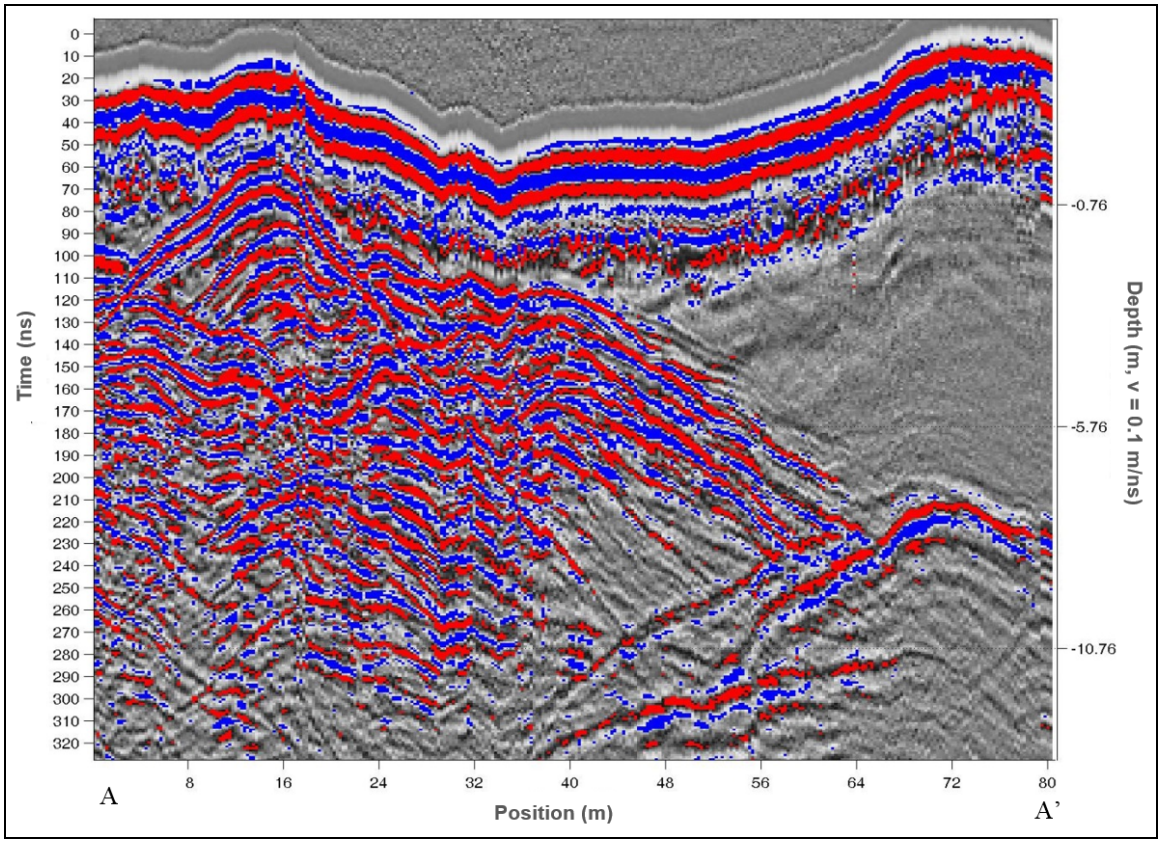

Figure 11. GPR profile of line 1.

Three reflectors were also present in Line 2. Located in the southern section of the slide (Figure 10), Line 2 was 84 m long and penetrated to a depth 12 m near the beginning and a depth of 9 m toward the end (Figure 13). The first reflector was a weak reflector visible from the beginning of the line and ending at a distance of 75 m (Figure 14). It was somewhat concave in shape with a maximum thickness of 10 m. The second reflectors were medium strength, beginning at a depth of 4 m near the start of the line and ending at a depth of 8 m 40 m along. The third reflector began at 40 m distance at a depth of 8 m and rose to near the surface at the end of the line.

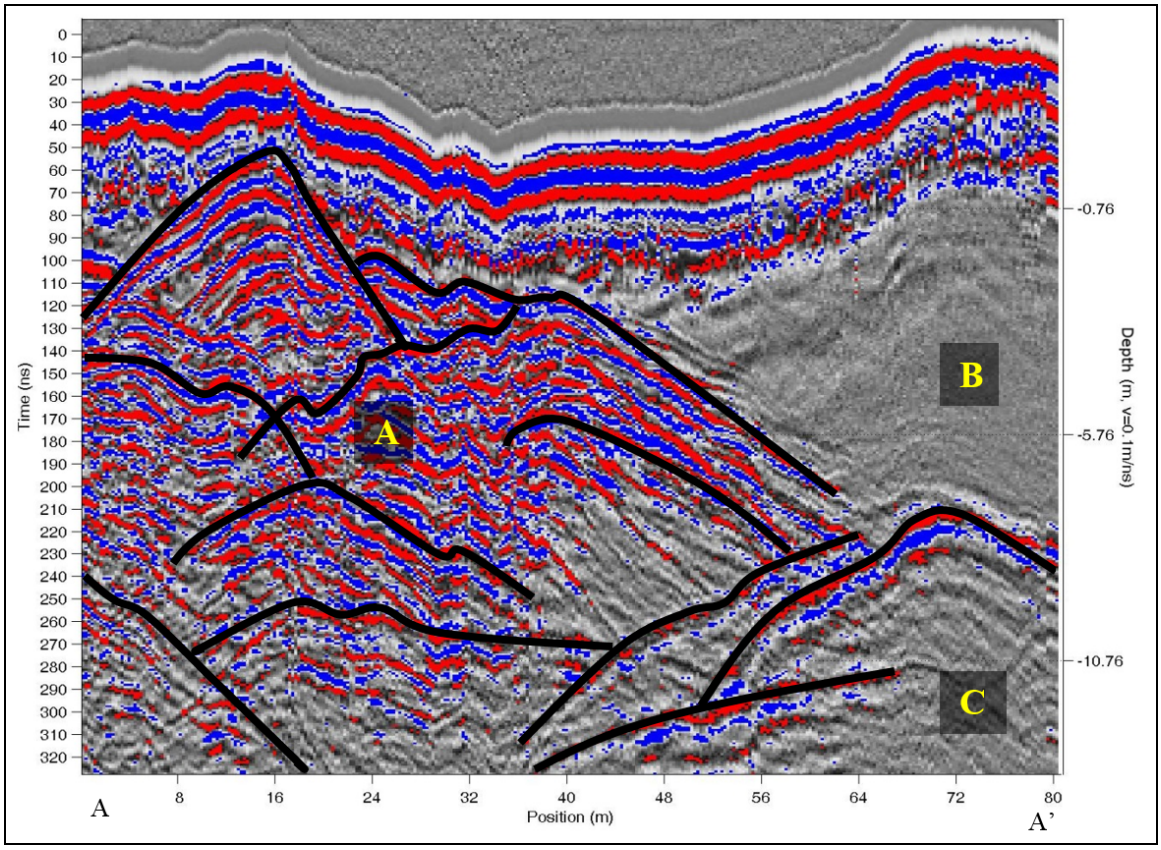

Figure 12. GPR profile of line 1 with highlighted subsurface features. (A) Represents the strong reflectors, (B) represents the weak reflectors and (C) represents the medium reflectors.

Line 3, located in the northern section of the study area (Figure 10), transected the graben across the landslide. This line was 56 m long and penetrated approximately 15 m deep at the start of the line to 12 m deep near the end (Figure 15). There were two types of reflectors on this line. The first was a small wedge of weak reflection at the beginning of the line near the surface with a thickness of approximately 2 m and a length of 9 m (Figure 16). The second reflector was strong and chaotic and encompassed most of the line. The reflection gradually declined in strength to medium reflections at depth. There was no distinct separation between the medium and strong reflections. There was

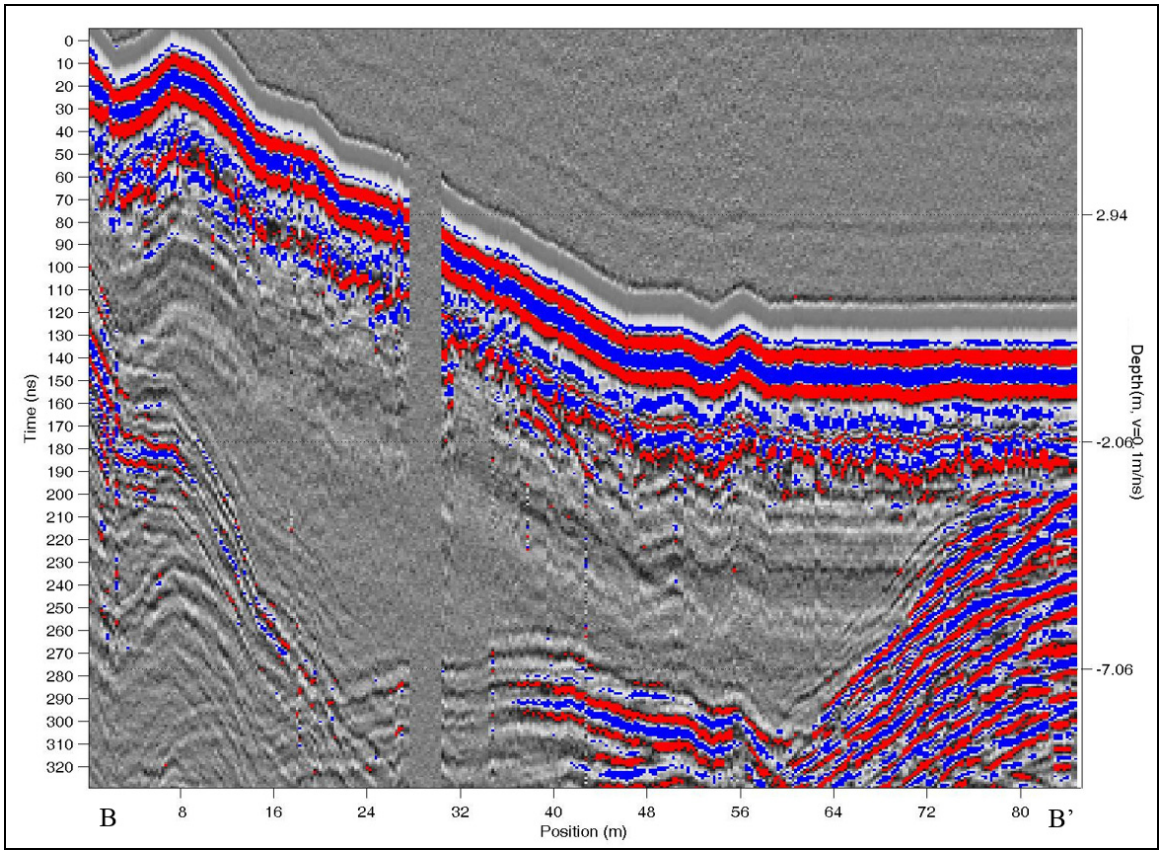

Figure 13. GPR profile of line 2.

significant interference on this line most likely caused by uneven terrain causing the quality of the reflections to be inferior.

Ground penetrating radar data were topographically corrected and interpreted according to knowledge of the site geology and accepted principles. Weak reflections seen in all of the surveys were interpreted as colluvium. Weak reflectors and small homogenous sections within valley fill most likely represent the result of erosion from the hillslope. The medium reflections seen in lines 1 and 2 were interpreted as Chico Formation. The reflections are parallel and consistent with thinly bedded sandstone seen in the study area, primarily within the Big Chico Creek channel. The strong reflections

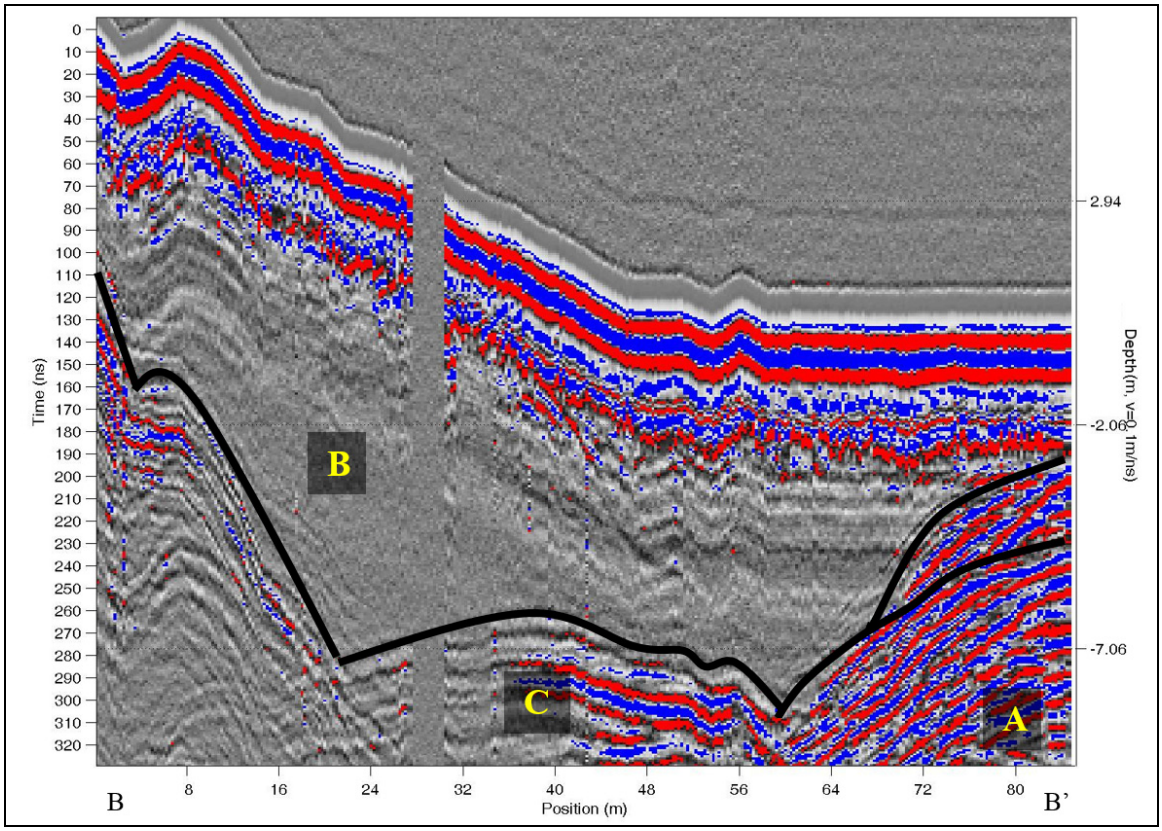

Figure 14. A GPR profile of line 2 with highlighted subsurface features. (A) Represents the strong reflectors, (B) represents the weak reflectors and (C) represents the medium reflectors.

could not be positively identified but exhibit chaotic reflections and interbedding characteristic of alluvial deposits. The strong parabolic reflection above the alluvium is characteristic of debris flows (Starheim et al. 2013) which are a main component of alluvial deposition. It is believed the origins of these deposits are a combination of Chico and Tuscan formations. It should be noted that the extremely strong reflections at the surface of each of the lines are caused by the direct waves from transmitter to the receiver. Just below these are somewhat scattered linear reflections caused by the multiple reflections of electromagnetic waves at the ground surface. If the contrast in

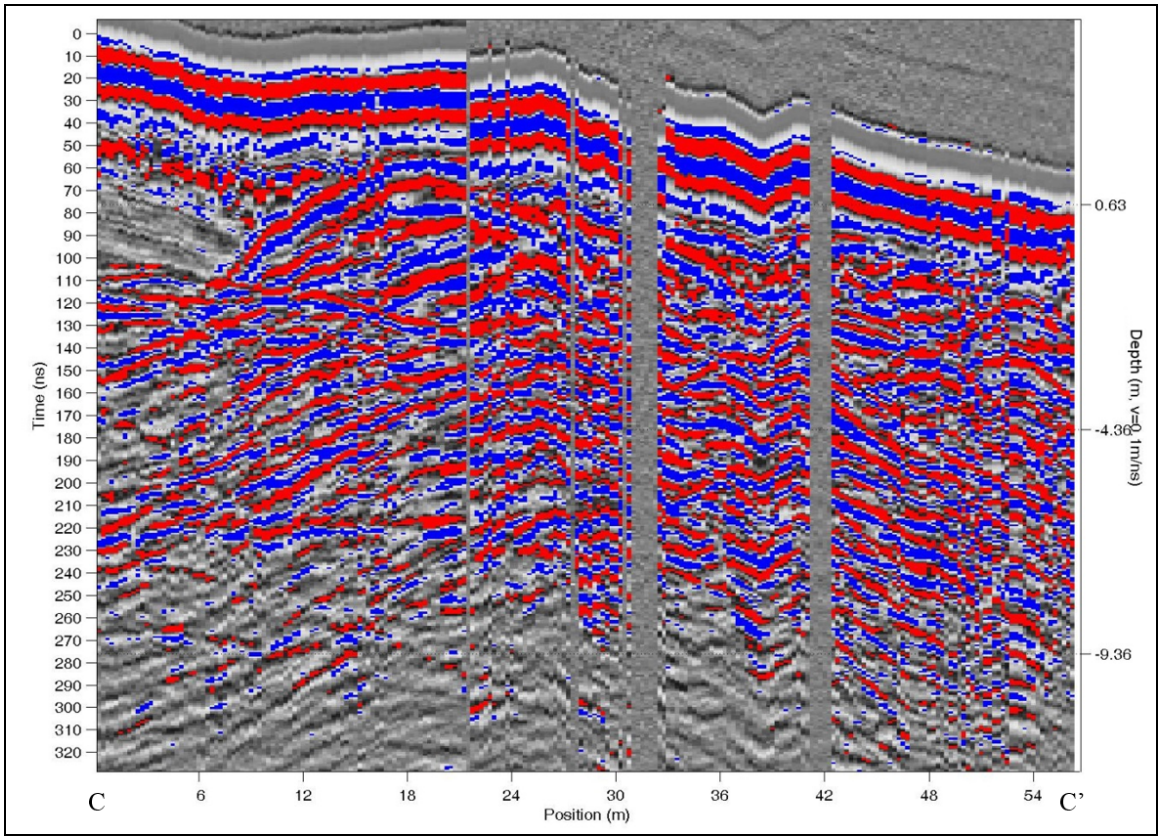

Figure 15. GPR profile of line 3.

impedance at the boundary is large, it can cause interpretation problems especially in marine sedimentary environments (Robinson and Çoruh, 1988).

According to these guidelines, Line 1 showed the strong parabolic signature of the debris flow and alluvium (Figure 17). The debris flow is approximately 18 m wide and sits upon the alluvial deposits. The contact between the colluvium and the Chico Formation can be seen between 38 and 80 m. Because some faults in ground penetrating radar surveys are seen as one-sided diffractions (Bano et al., 2000). A single dipping parabolic arm visible in the survey could suggest the presence of a micro-fault. Although near the contact, the reflection cuts across reflections parallel with the alluvial deposits.

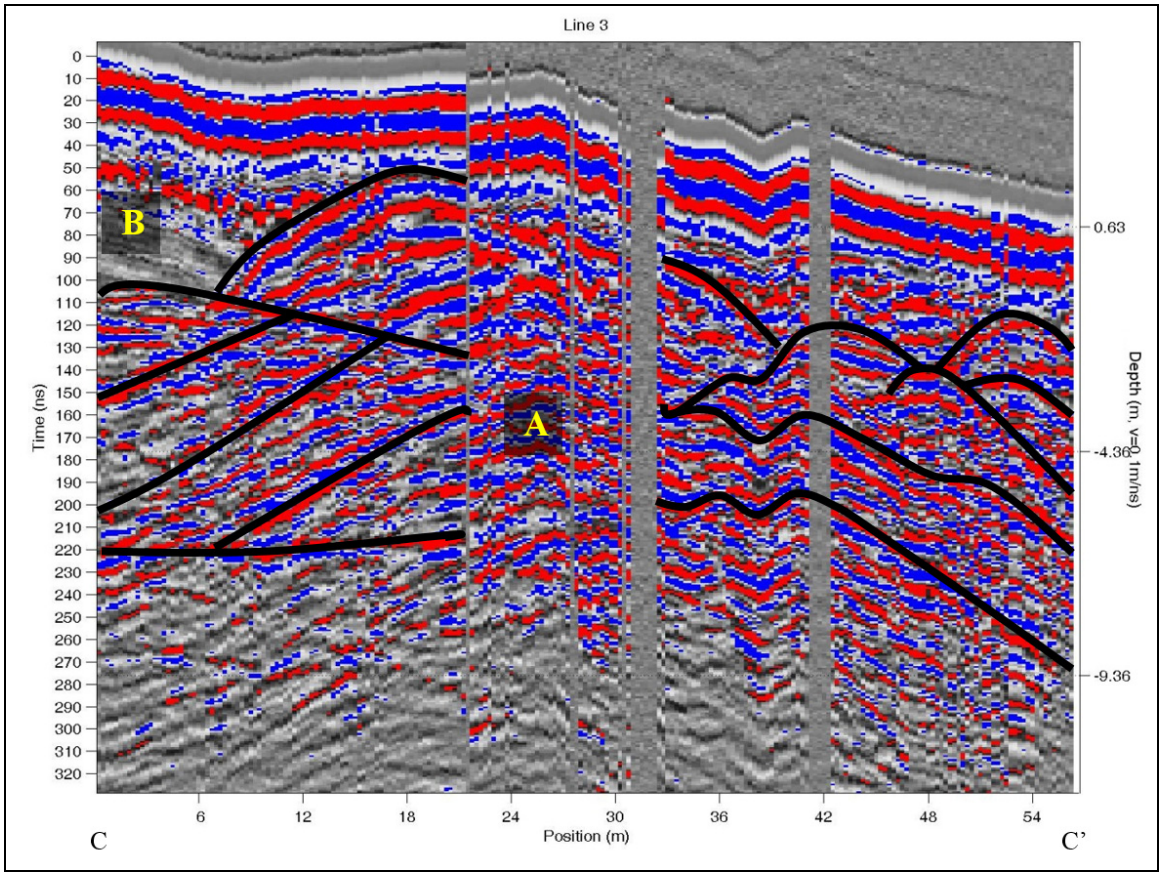

Figure 16. GPR profile line 3 highlighting selected features. (A) represents the strong reflectors and (B) represents the weak reflectors.

The GPR survey suggests Line 2 is composed of mostly colluvium. A 10-meter thick section of Chico Formation can be seen thinning to 2 m when it contacts another section of Chico Formation at 20 m. These both exhibit medium parallel reflections consistent with the other lines. At 60 m alluvial deposits can be seen (Figure 18).

Reflectors along Line 3 suggest the presence of alluvium with the debris flow from line 1 evident between 8 m and 26 m and a small amount of colluvium (Figure 19). There is evidence of alluvial deposits dipping to the north east between 0 m and 28 m

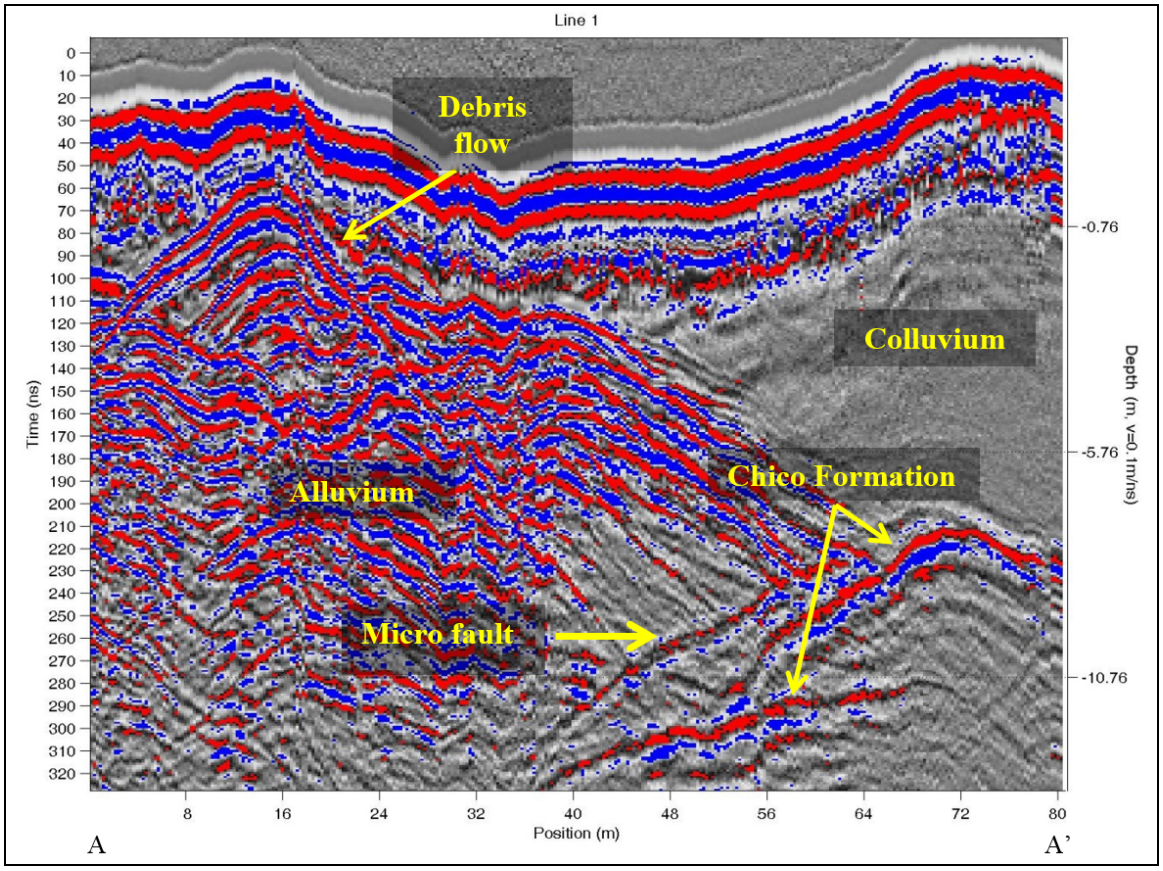

Figure 17. GPR profile of line 1 with interpreted features.

indicating possible channel migration. Beyond 26 m distortion in the line makes interpretation difficult. Thick grass along the line reduced contact with the ground surface and multiple terracettes in the graben may have contributed to uneven antenna spacing causing a poor quality reflection.

The magnitude and direction of periodic movement of the failed mass were assessed by installing pairs of survey flags in five different sections of the slide graben (Figure 20). Flag placement was dictated by access to the graben; pairs of survey flags were placed as evenly as possible across the graben to accurately capture movement. Within each pair, one survey flag was placed above the graben and one at the base of the

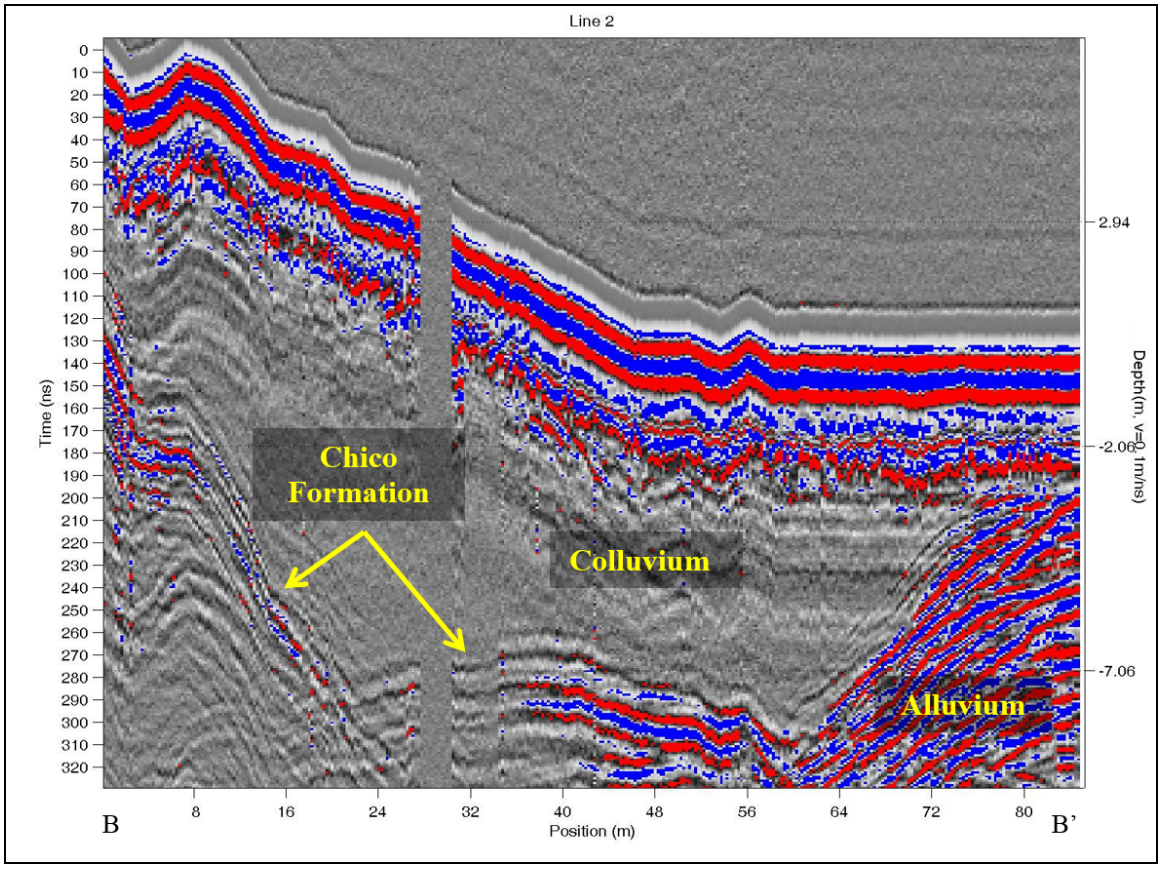

Figure 18. GPR profile line 2 showing interpreted features.

graben. The distance between the two survey flags at each of the five locations was measured using a measuring tape and a level to ensure accurate measurements. Both horizontal and vertical measurements between the two survey flags at each of the five locations were made.

Distances between flags were periodically measured between October 3, 2009 and August 29, 2010 (Table 2). At the end of the study period, the measurements between subsequent days were subtracted to determine if horizontal and vertical movement had occurred. Movement data acquired in this manner were largely inconclusive. While most of the measurements indicated that the distance between the flags increased, suggesting

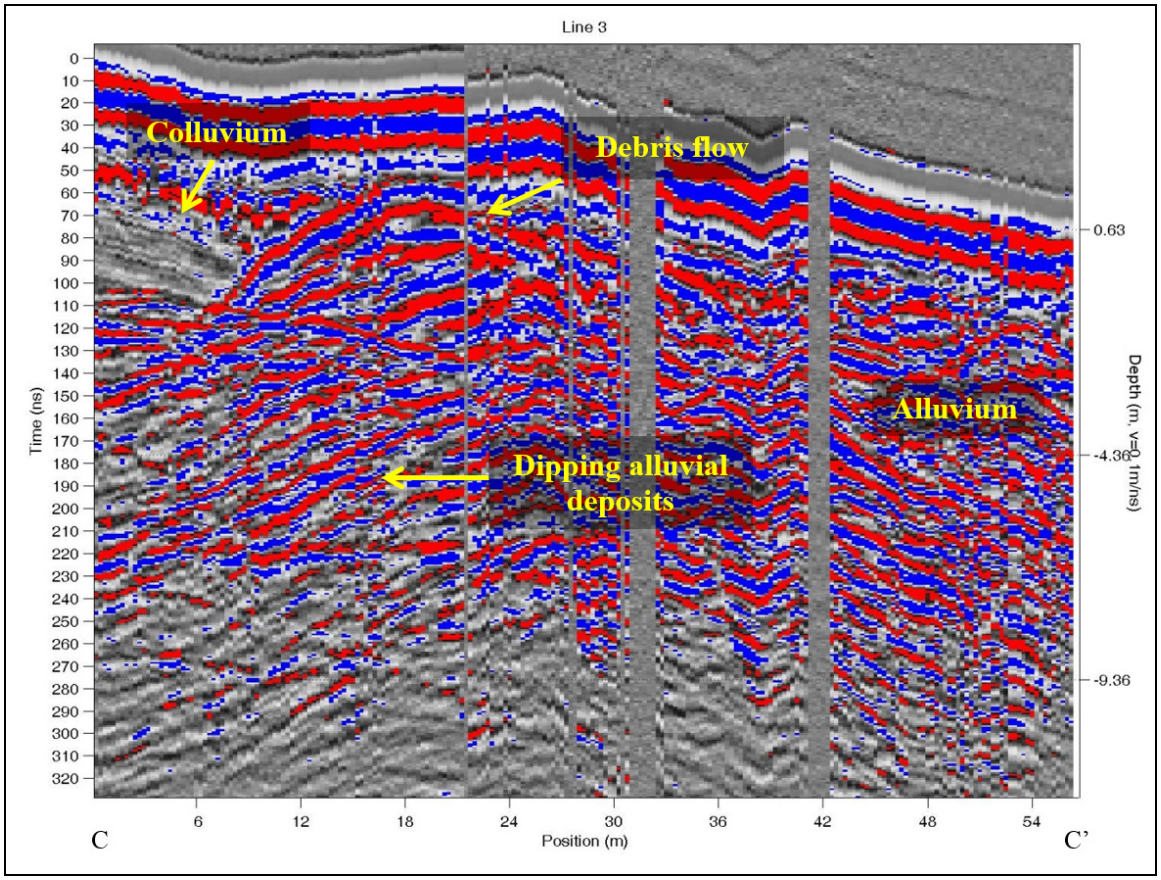

Figure 19. GPR profile line 3 showing interpreted features.

that the failure was moving downslope, some of the measurements indicated backward movement because the distance between flags decreased. The most probable cause of the appearance of backward movement was vegetal growth. The grasses that the survey flag pairs were placed in were thick and varied in height and thickness throughout the monitored seasons causing flag displacement.

Average rates of movement for each pair of flags in the graben (Figure 20) were calculated to determine if, overall, measurements indicated downslope movement even though some of the individual measurements indicated backward movement. Movement rates were calculated by dividing the change in distance by the time between

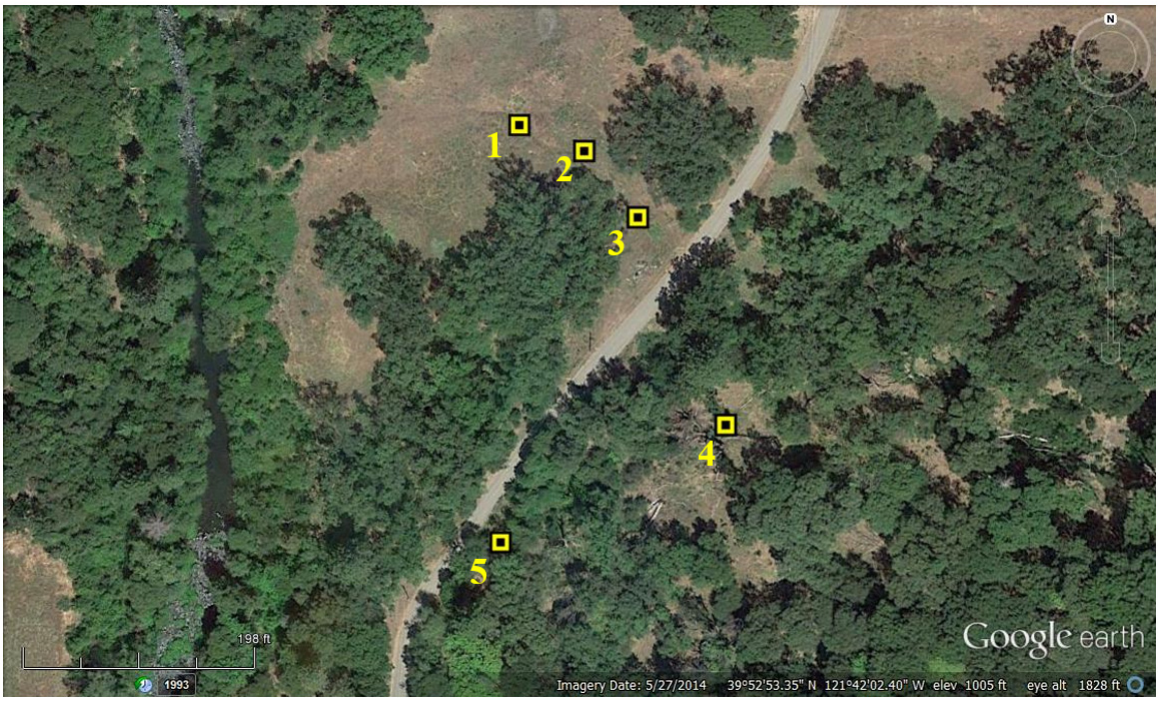

Figure 20. Satellite photo showing survey flag locations.

Source: "Flag locations." 39°52'53.35" N and 121°42'02.40" W. **Google Earth.** May 27, 2014. October 08, 2014**.**

measurements. These were then averaged for each measurement location to obtain the average rate of movement (Table 3). A positive value of movement in the horizontal direction indicated that the graben had moved apart, while a positive value in the vertical direction indicated that the graben had dropped down. These two values together indicated if the failure moved downslope. The recorded rates of movement were very small and indicated that if movement had occurred, it was extremely slow. The results indicate that the monitoring method was not sensitive enough to accurately capture the displacement of the failure data.

Because the initial flag measurements were inconclusive, the field area was revisited four years after the study concluded to determine if the area was actively

TABLE 2. MOVEMENT MEASUREMENTS BETWEEN SURVEY FLAG PAIRS

	Flag Number									
	1		2		3		4		5	
Date	Horizontal	Vertical	Horizontal	Vertical	Horizontal	Vertical	Horizontal	Vertical	Horizontal	Vertical
10/3/2009	24.1	47.6	75.6	120.0	30.5	66.0	203.2	262.6	74.9	101.6
11/14/2009	24.1	48.3	74	120.0	30.5	66.0	203.2	241.3	74.9	102.9
1/10/2010	24.8	48.3	74.9	120.7	29.21	67.3	200.7	238.8	76.2	102.9
2/14/2010	21.6	47.0	69.9	120.7	35.6	55.9	185.4	243.8	88.9	100.3
4/17/2010	22.2	47.0	69.9	127.6	33.0	57.8	195.6	247.7	83.8	109.2
5/2/2010	23.5	47.0	69.9	127.6	31.75	60.3	199.4	248.9	82.6	111.8
8/29/2010	Animal Disturbance		68.6	132.1	38.1	60.3	198.1	250.2	90.2	114.3
	Distance (cm)									

TABLE 3. AVERAGE RATES OF MOVEMENT BETWEEN SURVEY FLAG PAIRS AT EACH OF THE FIVE LOCATIONS

	Average Movement (cm/yr)	
Flag Number	Horizontal	Vertical
1	0.7	-0.3
2	-1.7	2.5
3	0.9	-1.1
4	-0.8	2.2
5	2.8	2.7

moving. Previous studies indicate using stakes in the ground to measure tilt can be an effective way to judge movement direction (Wieczorek and Snyder, 2009); consequently the degree and the direction of tilt of the piezometers were measured using a Brunton pocket transit (Table 4). The tilt measurements indicate that the direction of movement on

TABLE 4. PIEZOMETER TILT AND DIRECTION OF TILT

Piezometer #	Tilt	Direction of Tilt
1	4°	S10°W
2	3°	S35°W
3	5°	S5°W
4	0°	0
6	11°	S75°W

the steeper slopes was downslope toward Big Chico Creek. On the more gentle slopes, tilt measurements indicated movement downslope but somewhat parallel to Big Chico Creek (Figure 21). Piezometers 1 and 2 were tilted at an angle similar to the slope of the surrounding area. Piezometer 3 exhibited a tilt similar to that of the slope; however, the direction of tilt differed from the direction of slope by 55°. Piezometer 4, which is just outside the slide area to the north, was still level despite being on a 15° slope. Piezometer 5 could not be measured as it had been buried by debris from a fallen oak tree.

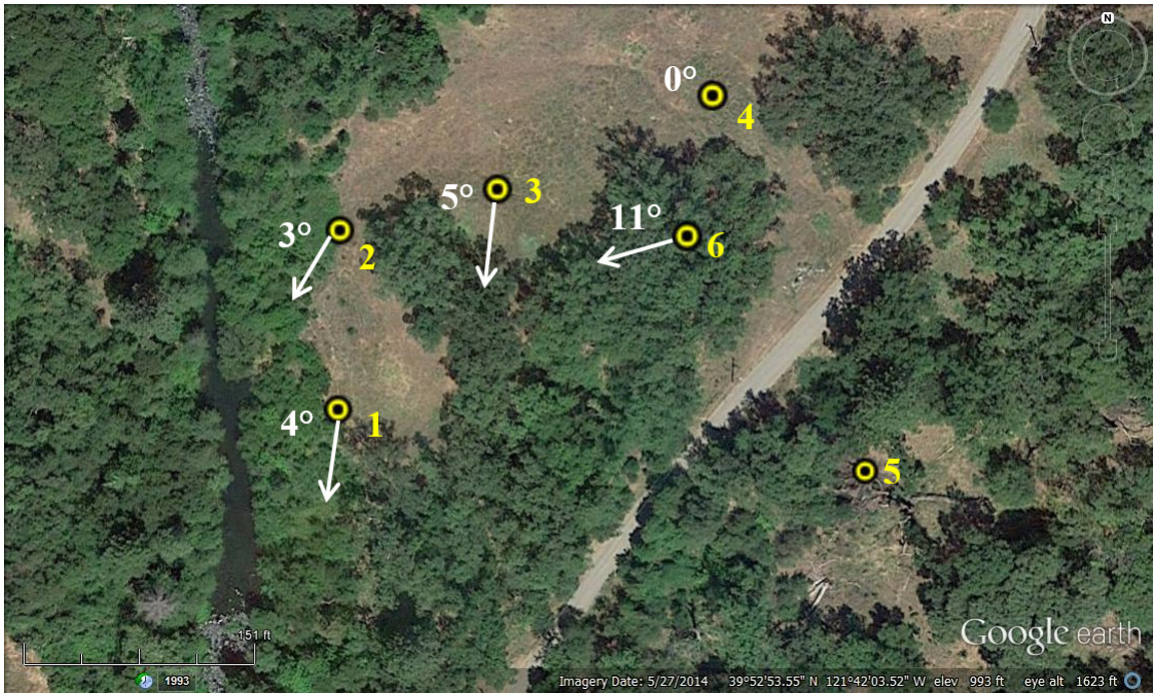

Figure 21. Satellite photo showing piezometer locations (yellow) with tilt measurements (white).

Source. "Tilt measurements." 39°52'53.55" N and 121°42'03.52" W. **Google Earth**. May 27, 2014. October 07, 2014.

Piezometer 6 exhibited by far the most tilt but was also on the steepest slope of all the piezometers (Figure 21).

CHAPTER IV

ANALYSIS AND DISCUSSION OF RESULTS

The objective of this study was to determine the conditions resulting in periodic slope instability on gently sloped terrain. It was hypothesized that that a perched water table, generated by excessive or intense precipitation events, affects the slope stability in the area and results in intermittent movement of the landslide. Data-gathering activities included monitoring precipitation, measuring the height and extent of the perched water table using a piezometer array, on-the-ground mapping of surface topographic features, interpreting the location and morphology of impermeable boundaries with ground-penetrating radar and assessing relative slide movements. Field measurements suggest that there is a correlation between the amount of rainfall received and the change in height of the rise of water above the impermeable surface; a slope-stability analysis was performed to quantify probable conditions resulting in stability.

The strength of the relations between precipitation volumes and the response of the perched water table were assessed using linear regression and cross-correlation analyses. Correlation between the total volume of the each significant precipitation event and the change in rise of the water level in each of the piezometers was determined by fitting a linear regression to the data points for each of the piezometers (Figure 22). Piezometers 2 and 3 exhibited the highest correlations with correlation coefficients of

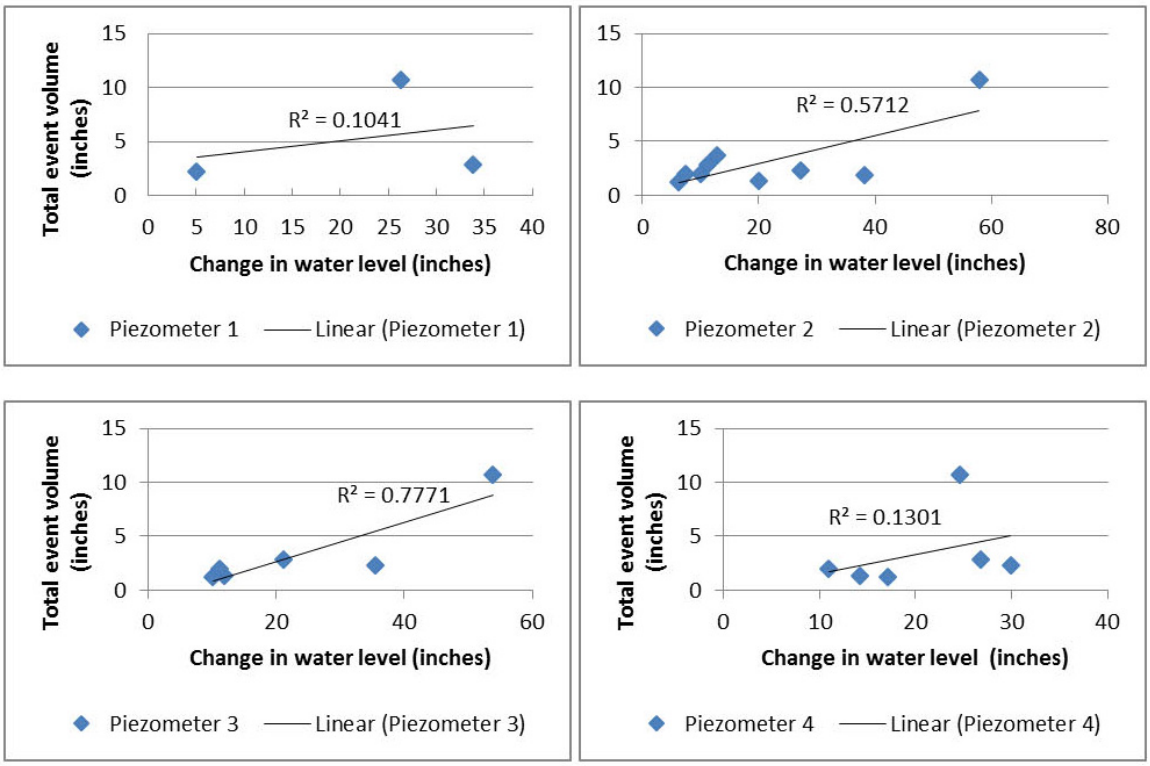

Figure 22. Graphs depicting the correlation between the total precipitation event volumes and the change in water level in piezometers 1-4.

0.75 and 0.88. Much lower correlation coefficients of 0.32 and 0.36 were exhibited by piezometers 1 and 4, respectively. The strong correlation between the volume of precipitation and the change in rise of the water level in Piezometers 2 and 3 is probably the result of piezometer location with respect to slide surface topography. Both piezometers were located at the base of slope beaks, Piezometer 2 on the east near the creek and Piezometer 3 near the center of the failure (Figure 4); these locations captured more runoff and allowed for more infiltration. In support of this theory is the observation that Piezometer 3 showed a response before the other piezometers during many of the precipitation events having shorter response times than the lower piezometers in the landslide (Figure 24) suggesting subsurface flow from upslope may be partially

responsible for the rapid rise in water level in the piezometer. Weak correlation between the volume of precipitation and the change in rise of the water level in Piezometers 1 and 4 can also be attributed to their locations; Piezometer 1 is in a hummock in the south east section of the failure and piezometer 4 is on a 15° slope outside of the failure (Figure 4). The location of the piezometers on high ground and a 15° slope resulted in poor correlation due to precipitation running off and not infiltrating locally.

A cross-correlation analysis was applied to statistically determine the relative timing between significant precipitation events and the total height of the perched water table. Hourly precipitation intensities from the nine rainfall events that occurred between October 4, 2009 and October 3, 2010, were compared with hourly measurements of water table levels in the four piezometers. Lag times between peak rainfall intensity and high water level were calculated by shifting the hourly precipitation values until maximum correlation of precipitation and water table levels for the event was achieved. A maximum correlation coefficient of 0.74, with a time lag of 11 hours, was calculated for piezometer 4 during event 9 (Table 5). Even with the time lag, the statistical analysis suggested the there was only a weak correlation between rainfall intensity and water levels in the piezometers.

Precipitation events were then subdivided into shorter events and cross-correlation with water level data was repeated. Events during which there were periods of precipitation of less than one tenth of an inch preceded and followed by several hours of no precipitation were subdivided into shorter events. The portion of the event with no precipitation was removed and the corresponding hours of water level data were used in the calculation of the maximum correlation of precipitation and water table levels.

TABLE 1. CORRELATION COEFFICIENT, r, AND LAG TIMES OF PRECIPITATION EVENTS FOR PIEZOMETERS 1-4

	Piezometer 1		Piezometer 2		Piezometer 3		Piezometer 4	
	r	Lag time	r	Lag time	r	Lag time	r	Lag time
Event 1	n/a	n/a	0.71	10	n/a	n/a	n/a	n/a
Event 2	n/a	n/a	0.49	11	n/a	n/a	n/a	n/a
Event 3	n/a	n/a	0.17	6	n/a	n/a	n/a	n/a
Event 4	0.46	6	0.19	14	0.07	6	0.21	5
Event 5	0.42	8	0.11	9	0.15	9	0.14	9
Event 6	n/a	n/a	0.65	15	0.73	9	0.69	13
Event 7	n/a	n/a	0.46	5	0.72	4	0.48	5
Event 8	0.54	21	0.59	21	0.57	21	0.57	21
Event 9	n/a	n/a	0.68	17	0.61	17	0.74	11

Correlations between precipitation and water levels in piezometers were stronger once a portion of the events were broken up into sub events (Table 6). Events 3a and 3b showed correlation coefficients in Piezometer 2 of 0.63 and 0.58, a significant increase from 0.17. The average lag time for this event was similar to the undivided event. Event 5 showed a

TABLE 2. CORRELATION COEFFICIENT, r, AND LAG TIMES OF SUBDIVIDED PRECIPITATION EVENTS FOR PIEZOMETERS 1-4

	Piezometer 1		Piezometer 2		Piezometer 3		Piezometer 4	
	r	Time lag	r	Time lag	r	Time lag	r	Time lag
Event 1	n/a	n/a	0.71	10	n/a	n/a	n/a	n/a
Event 2	n/a	n/a	0.48	11	n/a	n/a	n/a	n/a
Event 3a	n/a	n/a	0.63	9	n/a	n/a	n/a	n/a
Event 3b	n/a	n/a	0.58	4	n/a	n/a	n/a	n/a
Event 4	0.46	6	0.19	14	0.07	6	0.21	5
Event 5a	0.57	7	0.76	9	0.79	9	0.79	9
Event 5b	0.69	8	0.63	15	0.68	4	0.69	5
Event 6	n/a	n/a	0.65	15	0.73	9	0.69	13
Event 7b	n/a	n/a	0.91	5	0.93	4	0.86	6
Event 8	0.54	21	0.59	21	0.57	21	0.57	21
Event 9	n/a	n/a	0.68	17	0.61	17	0.74	11

significant increase in correlation for Piezometers 2, 3, and 4. During event 5a the lag times were equal to the undivided event and the lag times for event 5b were significantly shorter. Event 7b showed the highest increase in correlation however the lag times remained the same. During events 3b and 5b lag times were significantly shorter due to high antecedent moisture conditions resulting from events 3a and 5a.

The results suggest that correlation between precipitation events and height of the perched water table is greatly influenced by periods of little to no precipitation within storm events. During periods of light precipitation, antecedent moisture conditions rise but not enough to cause a rise in the perched water table adversely affecting correlation. Consequently, the highest correlations occur when high antecedent moisture conditions are followed by high intensity precipitation and a subsequent dry period. For example, Event 7b followed event 7a by 7 hours and the time lag was short at 4, 5 and 6 hours for piezometers 3, 2 and 4 respectively (Figure 23). This event showed a strong correlation between the amount of precipitation and the water levels in the piezometers. Conversely, event 4 was a series of storms lasting 9.5 days with many periods of no precipitation followed by light precipitation. Because the storms were so close together, there was little correlation between the precipitation and the water-level rise in the piezometers (Figure 24).

However, much of the lack of strong correlation between precipitation volume and intensity and piezometric water level rise for most of the events probably resulted from the source of the precipitation data. Precipitation data used in the analysis were from the Cohasset weather station nearly six kilometers away. Spatial variability in precipitation volume and intensity would have a significant influence on the magnitude

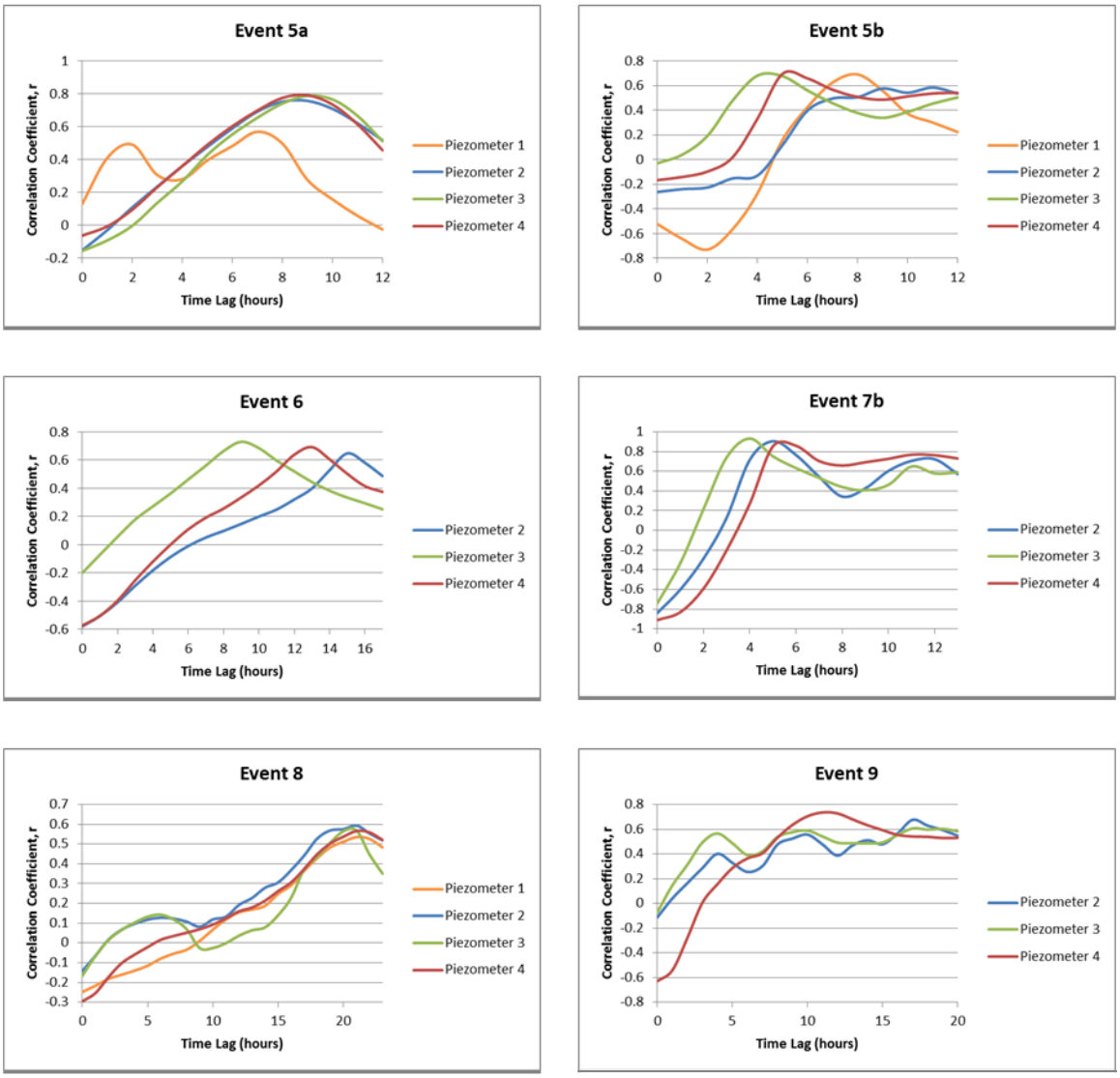

Figure 23. Correlation coefficient, r and time lag for precipitation events 5- 9.

and timing of the response in piezometers located in the study site. Although patterns between the magnitude and timing of precipitation and the relative response of the perched water table can be discerned, quantifying absolute values necessary for slope failure and correlating the magnitude of the water level rise with the accompanying degree of failure were not possible.

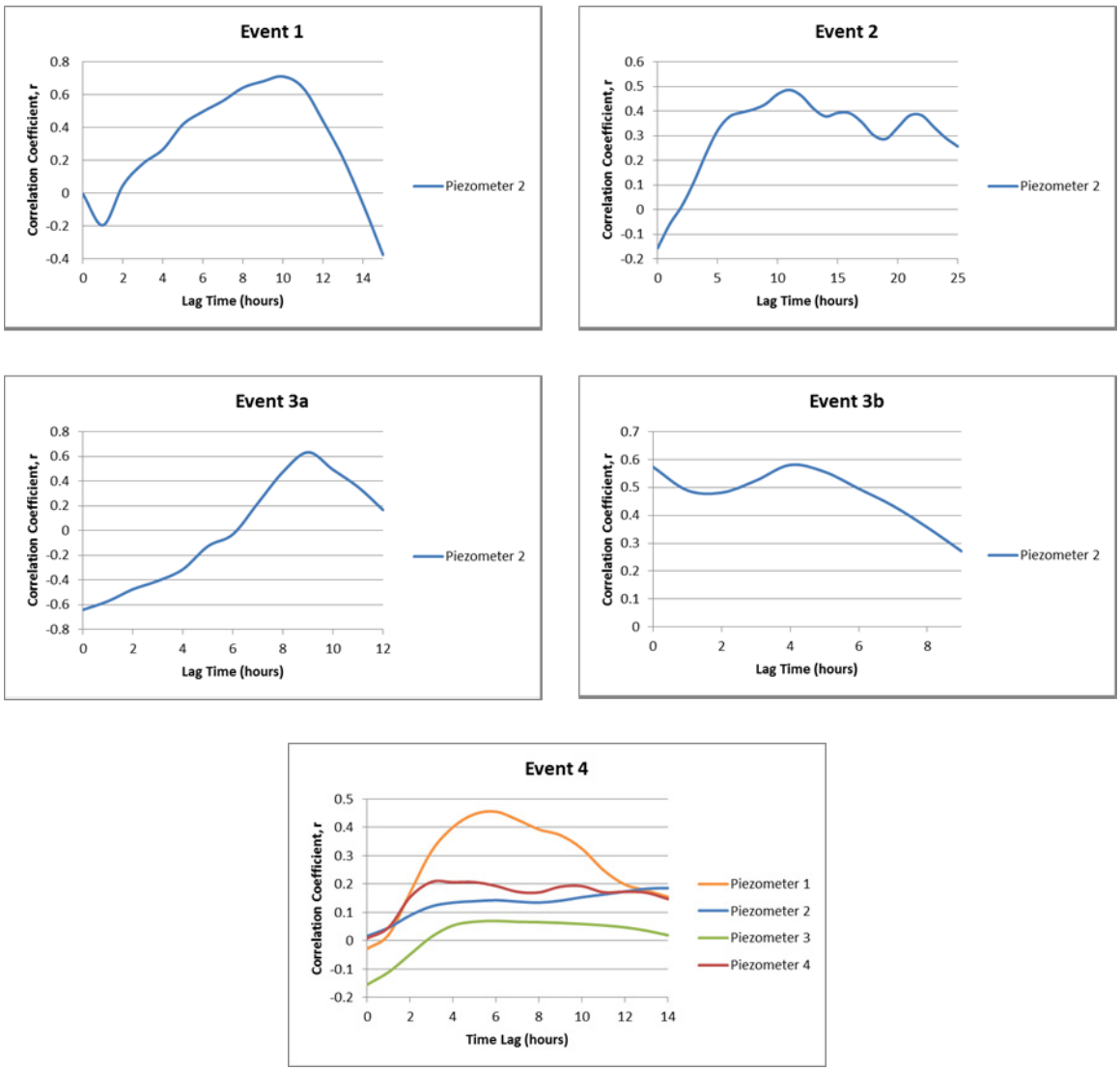

Figure 24. Correlation coefficient, r, and time lag for precipitation events 1-4.

Because conditions leading to slope instability and subsequent slope failure were only loosely quantified by field measurements, a factor of safety analysis was preformed to quantitatively assess conditions under which failure would occur. The factor of safety, F, is defined as

$$F = \frac{\text{Sum of the resisting forces (shear strength)}}{\text{Sum of the driving forces (shear stress)}}$$

Interpretation of the GPR data suggested that the failure surface is arcuate; therefore, the Swedish method of slices was used. First developed by Fellenius (1936), the method is widely applied in slope stability analysis (Selby, 1993). For this analysis, the form of the factor of safety equation used was

$$F = \frac{\sum[\, c'l + (W cos\alpha - ul) tan\phi']}{\sum[W sin\alpha]}$$

where:

c' = effective cohesion

l = length of base of slice

W = Area x 1m x γ (assuming a 1m thick slice)

α = angle of inclination

u = pore pressure

ϕ' = angle of friction with respect to effective stress

The surface topography was reconstructed based on field measurements. An arc was then fitted to the failure surface based on the depth of impermeable layers recorded in GPR transects and the failure divided into seven slices. The center of gravity and associated dropped vertical were then determined for each slice and a radius of the circle extended though the failure plane to determine α, the angle of inclination (Figure 25). From the figure, values for depth, z (m), length of the base, l (m), and area (m^2), could be measured. Slope, β, was determined on a per slice basis from topographic data used in the slope reconstruction.

Other parameters needed to run the model were obtained primarily from the literature. A combination of soils was present in the field area, including very fine sandy

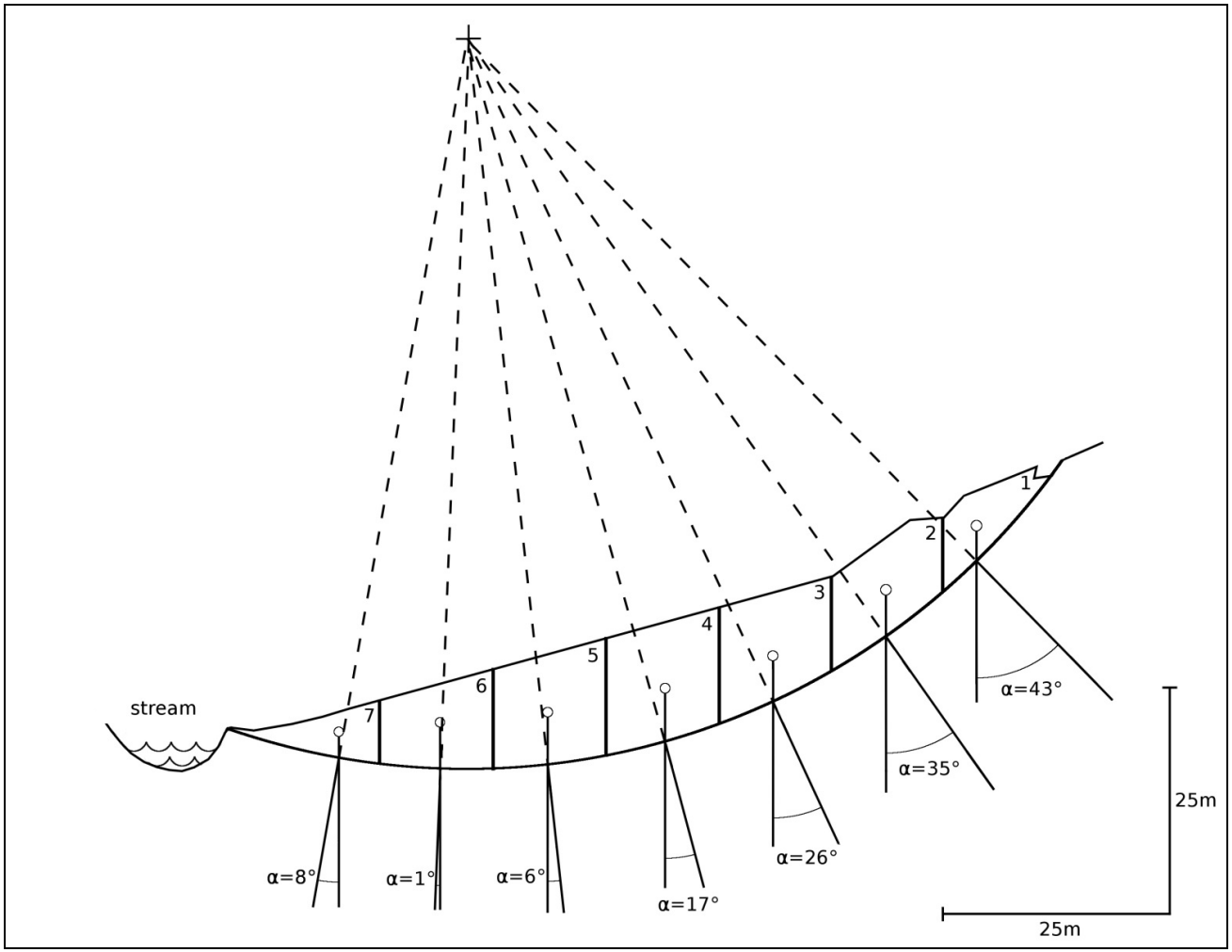

Figure 25. Swedish Method of Slices slope reconstruction and slice division.

loam and gravelly loam. Based on average percentages of sand, silt, and clay, deeper slide areas were determined to consist of a sandy clay loam (National Resources Conservation Service, 2012). Corresponding values for the effective cohesion, *c'* (10 kN/m^2) and the angle of internal friction with respect to effective stresses, ϕ' (34°), were obtained from the literature (geotechdata.info, 2013). The unit weight of soil at natural moisture conditions, γ (13.7 kN/m^3), was calculated using values for bulk density of the soil (USDA, 2008) and gravity. Pore water pressure, u, was calculated using the equation $u = \gamma_w mz\cos^2\beta$ where the pore pressure variance, m, represents the height of the perched water table above the impermeable surface divided by the depth of the slice. For a value of m = 1 the water table is at the ground surface, whereas for m = 0, the water table is just below the slide plane. For the purposes of this study m was varied to determine what fraction of saturated soil thickness above the slide plane would be needed for failure to occur. Slices 6 and 7 were assigned a negative driving force value because they were assumed to resist sliding (Appendix A).

The model was run several times to determine how high the perched water table needed to be to instigate slope instability. The results suggest that when the pore pressure variance, m, is equal to 0.5, the factor of safety, F, is equal to 1 (Figure 26). Perched water tables that sat at levels greater than half the distance up from the failure surface in the soil column would cause the slope to be unstable, while those sitting at less than half the distance would allow the slope to remain stable. Field measurements indicate that two of the piezometers in the lower section of the slide consistently showed the water table to be within 1 meter of the surface during and after precipitation events. For example, Piezometer 2, located near the creek, was within six inches of the ground

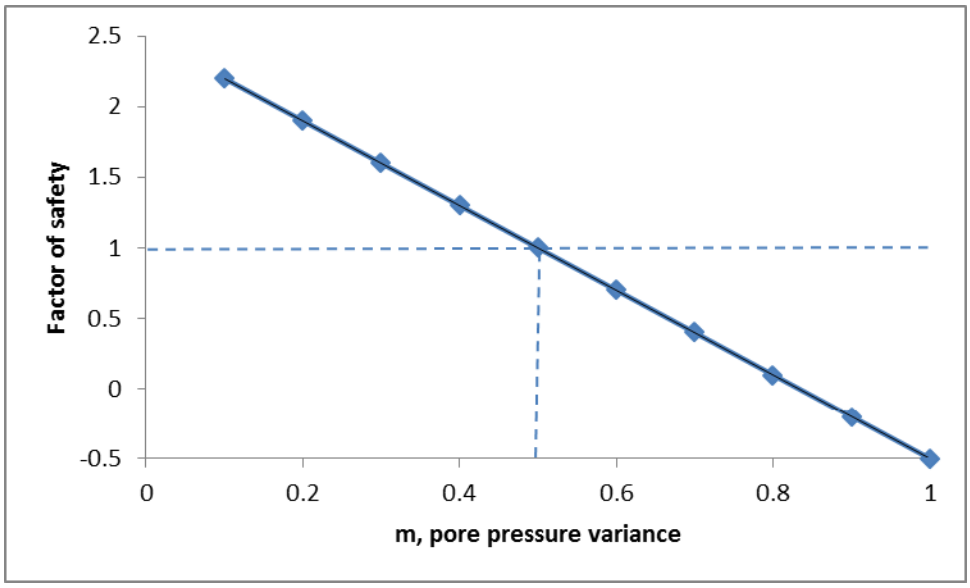

Figure 26. Variation in factor of safety as height of water table above the slide plane (m).

surface on several occasions and was within 1 m of the surface from January 13, 2010 to June 14, 2010 (Figure 6). Piezometer 3, located in the center of the failure, indicated that the water table was within 1 m of the ground surface from January 18, 2010 to May 22, 2010 (Figure 7) giving Piezometers 2 and 3 an m value of 0.9. Pore pressure variances greater than 0.5 were likely to result in slope instability, a condition common throughout the measured period.

CHAPTER V

CONCLUSIONS AND RECOMMENDATIONS

The results of the study indicate that intermittent instability of gentle slopes such as those in the study area ultimately depends on precipitation and the creation of a perched water table over an impermeable surface. In idealized models of slope instability, precipitation rates, infiltration rates, slope, depth to the impermeable layer and the level of the perched water table are all assumed to be constant and uniformly distributed. However, as reported in this study, other factors play a role in determining when and where the perched water table will form, thereby influencing the temporal and spatial variability of slope instability. These factors include variability in precipitation magnitude and intensity, and surface and subsurface topography.

Based on the findings of others (e.g., Torres et al., 1998), the initial hypothesis predicted that increases in the level of the perched water table would be governed largely by high intensity precipitation. However, it was found that the rise in the water table did not correlate with high intensity precipitation. The best correlation between precipitation and the formation and rise of a perched water table occurred when the total volume of the precipitation event was compared with the change in height of the water levels in the piezometers. The amount of precipitation needed to form a sustained perched water table during the monitored period was 11.8 inches; during the study, this amount was delivered

over a three-month period. Event 3 marked the beginning of a sustained perched water table in piezometer 2. While there were 30 days between precipitation events 2 and 3, there were several episodes of precipitation that were too small to be considered significant events preceding event 3 that would sufficiently increase antecedent moisture conditions.

The build-up of a perched water table was also dependent on surface topography and the location of impermeable layers. Piezometer placement, relative to the microrelief and slope, appeared to influence the formation and maintenance of a perched water table in every piezometer. Piezometer 1, for example, only responded to precipitation events after there was adequate antecedent soil moisture. While its position near the creek should have provided excellent evidence of a perched water table, it was located on a hummock. Piezometer 2 showed evidence of a perched water table before other piezometers and responded to all of the precipitation events; it was located at the bottom of the slope near the edge of the creek in a swale. Piezometer 3, located in the central lower section of the failure at the base of a slope break, was the second piezometer to form a perched water table. Piezometer 4 had the highest elevation and was located outside the failure on a 15° slope. A seasonal perched water table formed from January 25, 2010 to April 18, 2010. These observations suggest that any runoff generated by high intensity precipitation events would flow down steep slopes and collect at the base of the slopes or in swales, and allowing for increased infiltration in those areas and, adding to the build-up of a perched water table. Additionally, the GPR survey indicated that the field area is slightly concave. This concavity would funnel any surface or shallow

subsurface flow directly to the failure, also increasing the amount of water available for infiltration and build-up of a saturated layer.

The ground penetrating radar survey revealed impermeable layers in the subsurface that more or less mimic the general surface topography. Impermeable layers create somewhat of a bowl shape within the slide area, although the vertical extent of the bowl is obscured at the surface by alluvial and colluvial deposits. These deposits typically thicken in the middle of the slide area and thin towards the edges, where they are bounded by impermeable deposits on the east and west. This bowl shape tends to collect water draining from the surrounding hillslope and direct it into the center of the slide.

The seasonal perched water table began at the toe of the slope and extended upslope through time. Piezometer 2, located near the creek (Figure 4), maintained a perched water table from January 12, 2010 to July 1, 2010. Piezometer 3, located upslope and east of Piezometer 2, sustained a perched water table from January 18, 2010 to June 15, 2010, six days later than Piezometer 2. Piezometer 4, located just outside the failure and upslope to the north of Piezometers 2 and 3, maintained a perched water table from January 20, 2010 to April 26, 2010, 2 days after Piezometer 3. The water table receded, in the opposite direction, from Piezometer 4 through Piezometer 2, down slope.

Tilt measurements made after the study was concluded were used to infer the direction and magnitude of movement of the failed mass. It appears that the alluvial deposits and Chico Formation located around the edges of the slide prevent the failure from sliding directly down slope in to the creek and shifts the movement from a predominately western direction to the south, parallel to the creek. While timing of the movement could not be directly correlated with the formation and vertical fluctuation of

the perched water table, movement was occurring, albeit slowly. The average rates of movement calculated from field measurements (Table 3), although were largely inconclusive, were on the order of soil creep, which would be expected on gentle slopes. According to the factor of safety analysis, once the material above the impermeable layer was saturated to half of its vertical thickness, the slope would become unstable and slide until dewatering reduced the pore fluid pressure along the slide plane and the mass restabilized. Conditions resulting in the slow, downslope displacement of material are likely to occur every winter.

Several improvements to the study could be made to strengthen connections between slope instability and the conditions giving rise to it. A recording rain gauge located within the study site is essential to quantitatively defining the temporal correlation between precipitation magnitude and intensity and the creation and fluctuation of a perched water table. Expanding the piezometer array would allow correlation between timing of the rise of the perched water table, the position of the piezometers on the slide and the placement of the piezometers with respect to surface and subsurface topographic (including microrelief) features. A more sensitive surveying strategy, perhaps involving repeated surveys with precision equipment, is necessary to capture the slow, nearly imperceptible movement of the failed mass. Finally, detailed models of slide base mechanics could be applied to infer the physical circumstances governing movement and restabilization, providing greater insights into the conditions affecting instability on gentle slopes.

REFERENCES CITED

REFERENCES

Anderson, M. G., 1982, Modelling hillslope soil water status during drainage: Transactions of the Institute of British Geographers, v. 7, p. 337-353.

Bano, M., Marquis, G., Niviere, B., Maurin, J., and Cushing, M., 2000, Investigating alluvial and tectonic features with ground-penetrating radar and analyzing diffractions patterns: Journal of Applied Geophysics, v. 43, p. 33-41.

California Department of Water Resources, 2012, Cohasset (CST) station, California data exchange center: http://cdec.water.ca.gov/cgi-progs/staMeta?station_id=CST (June 2012).

Fellenius, W., 1936, Calculation of the stability of earth dams, *in* Transactions of the 2nd Congress on Large Dams, Washington, D.C.: International Commission on Large Dams (ICOLD), Paris, v. 4, pp. 445–462.

Freer, J., McDonnell, J. J., Beven, K. J., Peters, N. E., Burns, D. A., Hooper, R. P., Aulenbach, B., and Kendall, C., 2002, The role of bedrock topography on subsurface storm flow: Water Resources Research, v. 38, p. 1269.

Geotechdata.info, Angle of Friction, http://geotechdata.info/parameter/angle-of-friction.html (September 2013).

Geotechdata.info, 2013, Cohesion: http://geotechdata.info/parameter/cohesion (September 2013).

Leung, A. K., Sun, H. W., Millis, S. W., Pappin, J. W., Ng, C. W. W., and Wong, H. N., 2011, Field monitoring of an unsaturated saprolitic hillslope: Canadian Geotechnical Journal, v. 48, p. 339-353.

Olmsted, F. H., and Davis, G. H., 1961, Geologic features and ground-water storage capacity of the Sacramento Valley (Geological Survey water-supply paper 1497): http://pubs.usgs.gov/wsp/1497/report.pdf

Robinson, E. S., and Çoruh, C., 1988, Basic exploration geophysics: New York, New York: John Wiley & Sons, p. 562.

Selby, M. J., 1993, Hillslope materials and processes, 2d edition: Oxford: Oxford University Press, p. 480.

Sidle, R. C., and Swanston, D. N., 1982, Analysis of a small debris slide in coastal Alaska: Canadian Geotechnical Journal, v. 19, p. 167-174.

Soil Survey Staff, Natural Resources Conservation Service, United States Department of Agriculture, 2014, Web soil survey: http://websoilsurvey.nrcs.usda.gov/ (September 2014).

Soil Survey Staff, Natural Resources Conservation Service, United States Department of Agriculture, 2015, Web soil survey: http://websoilsurvey.nrcs.usda.gov/ (March 2015).

State of California, Department of Conservation, 2007, Interactive geologic map of the Chico quadrangle: California geological survey: http://www.quake.ca.gov/gmaps/RGM/chico/chico.html (June 2012).

Starheim, C. C.A., Gomez, C., Harrison, J., Kain, C., Brewer, N. J., Owen, K., Hadmoko, D. S., Purdie, H., Zawar-Reza, P., Owens, I., Wassmer, P., and Lavigne, F., 2013, Complex internal architecture of a debris-flow deposit revealed using ground-penetrating radar, Cass, New Zealand: New Zealand Geographer, v. 69, p. 26–38. doi: 10.1111/nzg.12002

Talebi, A., Uijlenhoet, R., and Troch, P. A., 2008, Application of a probabilistic model of rainfall-induced shallow landslides to complex hollows: Natural Hazards and Earth System Science, v, 8, p. 733-744.

Torres, R., Dietrich, W. E., Montgomery, D. R., Anderson, S. P., and Loague, K., 1998, Unsaturated zone processes and the hydrologic response of a steep, unchanneled catchment: Water Resources Research, v. 34, p. 1865-1879.

United States Geological Survey, September 2014, Landslides 101: http://landslides.usgs.gov/learn/ls101.php (September 2014).

USDA Natural Resources Conservation Service, June 2008, Soil quality indicators: http://www.nrcs.usda.gov/Internet/FSE_DOCUMENTS/nrcs142p2_053256.pdf (September 2014).

Weiler, M., McDonnell, J. J., Tromp-van Meerveld, I., and Uchida, T., 2006, Subsurface Stormflow. Encyclopedia of Hydrological Sciences. 10:112.

Wieczorek, G. F., and Snyder, J. B., 2009, Monitoring slope movements. Geololgical Monitoring, 245-271.

APPENDIX A

Factor of Safety Calculations

Slice	***c′***	***l***	***c′l***	***W***	**cos*α***	***Wcosα***	γ_w	***m***	***z***	$cos^2\beta$	***u***	***ul***	**tanφ′**	***c′l* + (*W*cosα-*ul*)tanφ′**	***sinα***	***Wsinα***
1	10	25	250	942.6	0.73	688.1	9.81	1	10	0.82	80.44	2011	0.67	-636.38	0.68	641
2	10	20.6	206	1799	0.82	1475	9.81	1	14.4	0.81	114.4	2357	0.67	-385.02	0.57	1025
3	10	17.5	175	2013	0.9	1811	9.81	1	15	0.92	135.4	2369	0.67	-198.77	0.44	885.5
4	10	16.3	163	2248	0.96	2158	9.81	1	16.9	0.92	152.5	2486	0.67	-56.69	0.29	652
5	10	15.6	156	2055	0.99	2034	9.81	1	15	0.92	135.4	2112	0.67	104.11	0.11	226.1
6	10	16.3	163	1519	1	1519	9.81	1	11.9	0.95	110.9	1808	0.67	-30.57	0.02	-36
7	10	21.3	213	663.1	0.99	656.5	9.81	1	6.9	0.99	67.01	1427	0.67	-303.50	0.14	-92.8
													Σ=	-1506.81	Σ=	3301
														F=	-0.46	

Slice	***c′***	***l***	***c′l***	***W***	**cos*α***	***Wcosα***	γ_w	***m***	***z***	$cos^2\beta$	***u***	***ul***	**tanφ′**	***c′l* + (*W*cosα-*ul*)tanφ′**	***sinα***	***Wsinα***
1	10	25	250	942.6	0.73	688.1	9.81	0.9	10	0.82	72.4	1810	0.67	-501.64	0.68	641
2	10	20.6	206	1799	0.82	1475	9.81	0.9	14.4	0.81	103	2121	0.67	-227.09	0.57	1025
3	10	17.5	175	2013	0.9	1811	9.81	0.9	15	0.92	121.8	2132	0.67	-40.04	0.44	885.5
4	10	16.3	163	2248	0.96	2158	9.81	0.9	16.9	0.92	137.3	2238	0.67	109.88	0.29	652
5	10	15.6	156	2055	0.99	2034	9.81	0.9	15	0.92	121.8	1901	0.67	245.61	0.11	226.1
6	10	16.3	163	1519	1	1519	9.81	0.9	11.9	0.95	99.81	1627	0.67	90.55	0.02	-36
7	10	21.3	213	663.1	0.99	656.5	9.81	0.9	6.9	0.99	60.31	1285	0.67	-207.86	0.14	-92.8
													Σ=	-530.59	Σ=	3301
														F=	-0.16	

Slice	***c′***	***l***	***c′l***	***W***	**cos*α***	***Wcosα***	γ_w	***m***	***z***	$cos^2\beta$	***u***	***ul***	**tanφ′**	***c′l* + (*W*cosα-*ul*)tanφ′**	***sinα***	***Wsinα***
1	10	25	250	942.6	0.73	688.1	9.81	0.8	10	0.82	64.35	1609	0.67	-366.90	0.68	641
2	10	20.6	206	1799	0.82	1475	9.81	0.8	14.4	0.81	91.54	1886	0.67	-69.16	0.57	1025
3	10	17.5	175	2013	0.9	1811	9.81	0.8	15	0.92	108.3	1895	0.67	118.69	0.44	885.5
4	10	16.3	163	2248	0.96	2158	9.81	0.8	16.9	0.92	122	1989	0.67	276.45	0.29	652
5	10	15.6	156	2055	0.99	2034	9.81	0.8	15	0.92	108.3	1690	0.67	387.10	0.11	226.1
6	10	16.3	163	1519	1	1519	9.81	0.8	11.9	0.95	88.72	1446	0.67	211.67	0.02	-36
7	10	21.3	213	663.1	0.99	656.5	9.81	0.8	6.9	0.99	53.61	1142	0.67	-112.23	0.14	-92.8
													Σ=	445.63	Σ=	3301
														F=	0.135	

Slice	***c′***	***l***	***c′l***	***W***	**cos*α***	***Wcosα***	γ_w	***m***	***z***	$cos^2\beta$	***u***	***ul***	**tanφ′**	***c′l* + (*W*cosα-*ul*)tanφ′**	***sinα***	***Wsinα***
1	10	25	250	942.6	0.73	688.1	9.81	0.7	10	0.82	56.31	1408	0.67	-232.16	0.68	641
2	10	20.6	206	1799	0.82	1475	9.81	0.7	14.4	0.81	80.1	1650	0.67	88.77	0.57	1025
3	10	17.5	175	2013	0.9	1811	9.81	0.7	15	0.92	94.76	1658	0.67	277.42	0.44	885.5
4	10	16.3	163	2248	0.96	2158	9.81	0.7	16.9	0.92	106.8	1740	0.67	443.03	0.29	652
5	10	15.6	156	2055	0.99	2034	9.81	0.7	15	0.92	94.76	1478	0.67	528.60	0.11	226.1
6	10	16.3	163	1519	1	1519	9.81	0.7	11.9	0.95	77.63	1265	0.67	332.78	0.02	-36
7	10	21.3	213	663.1	0.99	656.5	9.81	0.7	6.9	0.99	46.91	999.2	0.67	-16.60	0.14	-92.8
													Σ=	1421.85	Σ=	3301
														F=	0.431	

Slice	***c′***	***l***	***c′l***	***W***	**cos*α***	***Wcosα***	γ_w	***m***	***z***	$cos^2\beta$	***u***	***ul***	**tanφ′**	***c′l* + (*W*cosα-*ul*)tanφ′**	***sinα***	***Wsinα***
1	10	25	250	942.6	0.73	688.1	9.81	0.6	10	0.82	48.27	1207	0.67	-97.42	0.68	641
2	10	20.6	206	1799	0.82	1475	9.81	0.6	14.4	0.81	68.65	1414	0.67	246.69	0.57	1025
3	10	17.5	175	2013	0.9	1811	9.81	0.6	15	0.92	81.23	1421	0.67	436.15	0.44	885.5
4	10	16.3	163	2248	0.96	2158	9.81	0.6	16.9	0.92	91.52	1492	0.67	609.60	0.29	652
5	10	15.6	156	2055	0.99	2034	9.81	0.6	15	0.92	81.23	1267	0.67	670.10	0.11	226.1
6	10	16.3	163	1519	1	1519	9.81	0.6	11.9	0.95	66.54	1085	0.67	453.90	0.02	-36
7	10	21.3	213	663.1	0.99	656.5	9.81	0.6	6.9	0.99	40.21	856.4	0.67	79.04	0.14	-92.8
													Σ=	2398.07	Σ=	3301
														F=	0.726	

Factor of Safety Calculations

Slice	c'	l	$c'l$	W	cosα	$W\cos\alpha$	γ_w	m	z	$\cos^2\beta$	u	ul	tanφ'	$c'l + (W\cos\alpha - ul)\tan\varphi'$	$\sin\alpha$	$W\sin\alpha$
1	10	25	250	942.6	0.73	688.1	9.81	0.5	10	0.82	40.22	1006	0.67	37.32	0.68	641
2	10	20.6	206	1799	0.82	1475	9.81	0.5	14.4	0.81	57.21	1179	0.67	404.62	0.57	1025
3	10	17.5	175	2013	0.9	1811	9.81	0.5	15	0.92	67.69	1185	0.67	594.88	0.44	885.5
4	10	16.3	163	2248	0.96	2158	9.81	0.5	16.9	0.92	76.26	1243	0.67	776.17	0.29	652
5	10	15.6	156	2055	0.99	2034	9.81	0.5	15	0.92	67.69	1056	0.67	811.60	0.11	226.1
6	10	16.3	163	1519	1	1519	9.81	0.5	11.9	0.95	55.45	903.9	0.67	575.02	0.02	-36
7	10	21.3	213	663.1	0.99	656.5	9.81	0.5	6.9	0.99	33.51	713.7	0.67	174.67	0.14	-92.8
													Σ=	3374.29	Σ=	3301
														F=	1.022	

Slice	c'	l	$c'l$	W	cosα	$W\cos\alpha$	γ_w	m	z	$\cos^2\beta$	u	ul	tanφ'	$c'l + (W\cos\alpha - ul)\tan\varphi'$	$\sin\alpha$	$W\sin\alpha$
1	10	25	250	942.6	0.73	688.1	9.81	0.4	10	0.82	32.18	804.4	0.67	172.06	0.68	641
2	10	20.6	206	1799	0.82	1475	9.81	0.4	14.4	0.81	45.77	942.9	0.67	562.55	0.57	1025
3	10	17.5	175	2013	0.9	1811	9.81	0.4	15	0.92	54.15	947.6	0.67	753.61	0.44	885.5
4	10	16.3	163	2248	0.96	2158	9.81	0.4	16.9	0.92	61.01	994.5	0.67	942.75	0.29	652
5	10	15.6	156	2055	0.99	2034	9.81	0.4	15	0.92	54.15	844.8	0.67	953.09	0.11	226.1
6	10	16.3	163	1519	1	1519	9.81	0.4	11.9	0.95	44.36	723.1	0.67	696.13	0.02	-36
7	10	21.3	213	663.1	0.99	656.5	9.81	0.4	6.9	0.99	26.8	570.9	0.67	270.30	0.14	-92.8
													Σ=	4350.50	Σ=	3301
														F=	1.318	

Slice	c'	l	$c'l$	W	cosα	$W\cos\alpha$	γ_w	m	z	$\cos^2\beta$	u	ul	tanφ'	$c'l + (W\cos\alpha - ul)\tan\varphi'$	$\sin\alpha$	$W\sin\alpha$
1	10	25	250	942.6	0.73	688.1	9.81	0.3	10	0.82	24.13	603.3	0.67	306.80	0.68	641
2	10	20.6	206	1799	0.82	1475	9.81	0.3	14.4	0.81	34.33	707.1	0.67	720.48	0.57	1025
3	10	17.5	175	2013	0.9	1811	9.81	0.3	15	0.92	40.61	710.7	0.67	912.35	0.44	885.5
4	10	16.3	163	2248	0.96	2158	9.81	0.3	16.9	0.92	45.76	745.9	0.67	1109.32	0.29	652
5	10	15.6	156	2055	0.99	2034	9.81	0.3	15	0.92	40.61	633.6	0.67	1094.59	0.11	226.1
6	10	16.3	163	1519	1	1519	9.81	0.3	11.9	0.95	33.27	542.3	0.67	817.25	0.02	-36
7	10	21.3	213	663.1	0.99	656.5	9.81	0.3	6.9	0.99	20.1	428.2	0.67	365.94	0.14	-92.8
													Σ=	5326.72	Σ=	3301
														F=	1.614	

Slice	c'	l	$c'l$	W	cosα	$W\cos\alpha$	γ_w	m	z	$\cos^2\beta$	u	ul	tanφ'	$c'l + (W\cos\alpha - ul)\tan\varphi'$	$\sin\alpha$	$W\sin\alpha$
1	10	25	250	942.6	0.73	688.1	9.81	0.2	10	0.82	16.09	402.2	0.67	441.54	0.68	641
2	10	20.6	206	1799	0.82	1475	9.81	0.2	14.4	0.81	22.88	471.4	0.67	878.41	0.57	1025
3	10	17.5	175	2013	0.9	1811	9.81	0.2	15	0.92	27.08	473.8	0.67	1071.08	0.44	885.5
4	10	16.3	163	2248	0.96	2158	9.81	0.2	16.9	0.92	30.51	497.2	0.67	1275.90	0.29	652
5	10	15.6	156	2055	0.99	2034	9.81	0.2	15	0.92	27.08	422.4	0.67	1236.09	0.11	226.1
6	10	16.3	163	1519	1	1519	9.81	0.2	11.9	0.95	22.18	361.5	0.67	938.36	0.02	-36
7	10	21.3	213	663.1	0.99	656.5	9.81	0.2	6.9	0.99	13.4	285.5	0.67	461.57	0.14	-92.8
													Σ=	6302.94	Σ=	3301
														F=	1.909	

Slice	c'	l	$c'l$	W	cosα	$W\cos\alpha$	γ_w	m	z	$\cos^2\beta$	u	ul	tanφ'	$c'l + (W\cos\alpha - ul)\tan\varphi'$	$\sin\alpha$	$W\sin\alpha$
1	10	25	250	942.6	0.73	688.1	9.81	0.1	10	0.82	8.044	201.1	0.67	576.29	0.68	641
2	10	20.6	206	1799	0.82	1475	9.81	0.1	14.4	0.81	11.44	235.7	0.67	1036.33	0.57	1025
3	10	17.5	175	2013	0.9	1811	9.81	0.1	15	0.92	13.54	236.9	0.67	1229.81	0.44	885.5
4	10	16.3	163	2248	0.96	2158	9.81	0.1	16.9	0.92	15.25	248.6	0.67	1442.47	0.29	652
5	10	15.6	156	2055	0.99	2034	9.81	0.1	15	0.92	13.54	211.2	0.67	1377.58	0.11	226.1
6	10	16.3	163	1519	1	1519	9.81	0.1	11.9	0.95	11.09	180.8	0.67	1059.48	0.02	-36
7	10	21.3	213	663.1	0.99	656.5	9.81	0.1	6.9	0.99	6.701	142.7	0.67	557.20	0.14	-92.8
													Σ=	7279.16	Σ=	3301
														F=	2.205	